
Quantifying the Pre-training Dividend: Generative versus Latent Self-Supervised Learning for Time Series Foundation Models

Noam Major Kathy Razmadze Yoli Shavit*

Faculty of Engineering, Bar-Ilan University, Israel

Abstract

The success of self-supervised learning (SSL) in vision and NLP has motivated its rapid adoption for time series. However, research has focused primarily on Generative paradigms and forecasting tasks, leaving the broader utility of learned representations unquantified. We establish a controlled framework to evaluate the "pre-training dividend": the value added by SSL across diverse temporal tasks. We systematically compare Generative paradigms against Latent Alignment architectures, introducing adaptations of LeJEPa and DINO for time series. These adaptations utilize Discrete Wavelet Transform (DWT) augmentations to enforce invariance to local fluctuations. Our analysis reveals that the pre-training dividend is highly asymmetric: SSL yields gains of up to 375% for anomaly detection and classification, yet remains marginal for forecasting. We demonstrate that representational utility is non-universal, governed by a precision-invariance trade-off where the specific signal resolution required by the task must align with the objective. Finally, we show that representation quality is largely independent of data origin and saturates at moderate architectural depths, suggesting a path to scaling via massive synthetic generation. Our code is available at: <https://github.com/noammajor/Models>.

1 Introduction

The success of self-supervised learning (SSL) in natural language processing [17] and computer vision [4, 10] has motivated its widespread adoption for time-series analysis. However, temporal signals lack the discrete vocabularies or spatial hierarchies found in other domains; they are continuous, non-stationary, and often dominated by stochastic noise. Despite these distinctions, time series SSL has been largely evaluated through incremental gains in downstream forecasting [1, 5], leaving the broader utility of learned representations poorly understood.

This motivates a critical re-examination of SSL paradigms for time series analysis. Generative methods, such as Masked Auto-Encoding (MAE) [13], Diffusion Models [21] and Next Token Prediction (NTP) [5, 1], restore signals in the target domain but risk overfitting to local fluctuations. Conversely, Latent Alignment methods, such as invariance-based distillation (DINO) [4] and Joint-Embedding Predictive Architectures (JEPa) [10, 2], learn structural relationships in representation space but may collapse informative variability. To date, the lack of a principled comparison between these paradigms means the added value of SSL remains largely unquantified across diverse tasks.

In this work, we establish a controlled framework to address three central research questions:

RQ1. What is the added value of SSL across diverse time series task families?

*Corresponding Author. Email: yoli.shavit@biu.ac.il

RQ2. How does the choice of SSL objective dictate downstream performance?

RQ3. To what extent is representation quality driven by data origin and architectural scale?

To resolve these questions, we fix the backbone architecture and data pipeline to isolate the SSL objective as the primary variable. We evaluate Generative paradigms (NTP, MAE, Diffusion) alongside Latent Alignment methods (JEPA, LeJEPA, DINO). For methods which leverage augmented views (LeJEPA and DINO), we recognize that standard vision-based augmentations (e.g., cropping) often fail to respect temporal dependencies and propose enforcing frequency-domain invariance via Discrete Wavelet Transform (DWT). In our Wavelet-based DINO and Le-JEPA adaptations, the model aligns a Teacher view, generated via soft-thresholding of wavelet coefficients, with a "perturbed" Student view subjected to high-frequency noise and detail zeroing. By aligning these views in latent space, the model learns to remain invariant to local fluctuations while preserving the frequency components that define the system's state.

Our analysis reveals three fundamental properties of SSL for time series. First, the pre-training dividend is highly asymmetric. SSL establishes a robust foundation for anomaly detection and classification, but provides only marginal gains in forecasting. Second, representational utility is non-universal. Transferability depends on whether an objective preserves the signal resolution required by the downstream task. Latent Alignment paradigms prioritize global structural characteristics, which proves effective for morphological anomaly detection. However, a divergence emerges in classification: LeJEPA excels in linear probing while DINO proves superior under full fine-tuning. We hypothesize that the same mechanisms enabling LeJEPA's performance on semantic tasks also lead to its severe performance degradation in forecasting. Conversely, Generative paradigms prioritize the high-resolution fidelity necessary for granular anomaly detection, yet lack the semantic abstraction required for complex classification. Finally, we observe that data scale overshadows data origin, as pre-training on massive synthetic datasets achieves parity with real-world data, and that performance saturates at moderate architectural depths. Collectively, these findings suggest that current SSL methods are bottlenecked by their objective design and data scale, rather than model capacity, and that hybrid, paradigms and massive-scale synthetic data generation are promising directions.

In summary, our contributions are as follows:

- We introduce a unified and controlled benchmarking framework to quantify the added value of SSL across diverse time series task families, providing empirical answers to how different paradigms shape temporal representations.
- We propose a novel adaptation of Le-JEPA and DINO for time series SSL by introducing augmentations which are more suitable for temporal signals.
- We establish empirical scaling laws for temporal SSL, demonstrating that increasing architectural depth yields diminishing returns beyond a specific threshold under current regimes and showing that large-scale synthetic pre-training achieves parity with real-world data.

2 Related Work

2.1 Paradigms of Self-Supervised Learning in Time Series

We categorize the temporal SSL landscape by the pretext objective.

Generative Paradigms. These methods utilize signal-space alignment as a learning signal. Masked Auto-encoding (MAE), such as PatchTST [13] and SimMTM [6], reconstructs masked segments, while models like Chronos [1] and TimesFM [5] utilize Next-Token Prediction (NTP) and NTP-like objectives (forecasting) for continuous or quantized signals. Recently, diffusion-based frameworks like TimeDART [21] have introduced denoising objectives. While effective for forecasting, these paradigms risk overfitting to stochastic signal noise.

Latent Alignment Paradigms. Shifting the objective to the latent space, predictive approaches like JEPA [10] and invariance-based methods like DINO [4] align representations directly. This is critical for continuous time series, where reconstructive targets are highly susceptible to local fluctuations. Early explorations in this space include CPC [15], TS-JEPA [8], and TimeSiam [7]. We decouple the objective from proprietary architectures and focus on JEPA, LeJEPA [2] and DINO,

while introducing the necessary adaptations for time series analysis implemented through wavelets-based augmentations. We compare these augmentations to global/local view-based transformations, introduced for vision [4] and time series classification [12] in Appendix A.7.

Data Curation and Scaling. The field has moved from single-domain datasets toward multi-domain corpora like the Monash Archive [9]. Concurrently, synthetic data (e.g., Gaussian processes in Chronos [1] or TimePFN [16]) has emerged to enable zero-shot generalization. Our study investigates the interaction between these data sources and specific SSL objectives.

2.2 The Attribution Gap and Evaluation Biases

Existing surveys provide high-level taxonomies of contrastive and generative families [20, 22, 11], but lack a framework for isolating the specific impact of the pre-training objective. Furthermore, they do not cover emerging latent-alignment methods like DINO, JEPA and LeJEPA. Moreover, most temporal SSL research introduces new objectives alongside specialized architectures, creating an *attribution gap* where gains cannot be cleanly disentangled from architectural innovations. We address this by isolating the objective from data and architecture, covering both Generative and Latent paradigms while purposefully excluding contrastive methods (e.g., [19]) to eliminate confounding factors like negative sampling bias. In addition, SSL evaluation is dominated by forecasting benchmarks and zero-shot evaluations, providing a narrow assessment of representational utility. While libraries like TSLib [18] standardize implementations, they do not isolate pre-training variables. In this work we evaluate SSL methods via linear probing and full fine-tuning across diverse temporal tasks.

3 A Unified Framework to Compare SSL Paradigms for Time Series

We define a unified framework to compare Generative and Latent SSL paradigms. Let $\mathbf{x} \in \mathbb{R}^{T \times C}$ be a multivariate time series. Following the architectural principles in [13], we adopt a channel-independent approach, where each of the C channels is treated as an individual univariate series. To maintain a fair comparison, all paradigms utilize a Transformer backbone with the same capacity, and with paradigm-specific heads or decoders (dec_ϕ) added only where mathematically necessary. We denote this backbone as $f_\theta(\cdot)$, mapping the input to a latent representation $\mathbf{z} \in \mathbb{R}^{L \times D}$.

3.1 Generative Paradigms

Generative paradigms operate directly in the raw signal space, requiring the model to capture the exact numerical morphology and temporal dependencies of the data. We evaluate Next-Token Prediction (NTP) and Masked Autoencoders (MAE) as representatives of reconstructive and causal modeling, respectively, alongside Diffusion, which frames learning as a stochastic denoising process.

Masked Auto-Encoding (MAE): Following the patch-based strategy in [13], \mathbf{x} is divided into patches. A subset of patches \mathcal{M} is masked, and the model is trained to reconstructs the raw values through the Mean Squared Error (MSE) loss:

$$\mathcal{L}_{\text{MAE}} = \frac{1}{|\mathcal{M}|} \sum_{i \in \mathcal{M}} |\mathbf{x}_i - \hat{\mathbf{x}}_i|_2^2 \quad (1)$$

where $\hat{\mathbf{x}}_i$ is the output of the decoder at position i : $\phi(f_\theta(\mathbf{x}_{\setminus \mathcal{M}}))$ when applied to the visible patches $\mathbf{x}_{\setminus \mathcal{M}}$.

Next Token Prediction (NTP): We implement the work of TimesFM[5] to implement causal generation for a regression problem. Unlike traditional NTP, which relies on discrete token classification and autoregressive generation, this approach utilizes forecasting as a training surrogate to enforce directional temporal dependencies. At each position j , the model learns to predict a future forecast horizon of h patches based on the preceding context, by minimizing the MSE over the predicted horizon across all N windows:

$$\mathcal{L}_{\text{NTP}} = \frac{1}{N} \sum_{j=1}^N |\psi(f_\theta(\mathbf{x}_{1:p_j})) - \mathbf{x}_{p_j+1:p_j+h}|_2^2 \quad (2)$$

where f_θ is the causal backbone and ψ is the projection head.

Diffusion Models: We follow TimeDART [21] as a diffusion representative. The model learns to reverse a Gaussian corruption process. Given a noisy signal \mathbf{x}_t at timestep t , the model predicts the added noise ϵ via a denoising objective:

$$\mathcal{L}_{\text{Diff}} = \sum_{n=1}^{N-1} \mathbb{E}_{\epsilon, q(x_n)} [|\mathbf{x}_{n+1} - \phi(\hat{\mathbf{z}}_n^{in}, f_{\theta}(\mathbf{z}_{1:n}^{in}))|_2^2] \quad (3)$$

where $\hat{\mathbf{z}}_n^{in}$ denotes embeddings of the noise-added patch, and ϕ denotes a denoising decoder.

3.2 Latent Alignment Paradigms

In contrast to generative approaches, Latent Alignment Paradigms shift the learning objective to the feature space, where the goal is to align representations across different augmented or partial views of the same data. These methods can be broadly categorized into Joint-Embedding Predictive Architecture (JEPA)-based models, which learn to infer missing or augmented information within the latent space, and invariance-based models, which enforce consistency between augmented views through self-distillation. We evaluate JEPA and Le-JEPA as representative of the predictive paradigm and DINO as the primary representative of the invariance-based approach.

JEPA: In the Joint-Embedding Predictive Architecture (JEPA), the learning objective is to predict the representation of a target signal \mathbf{y} from a context \mathbf{x} entirely within the latent space. To prevent representational collapse without the use of negative pairs, an Exponential Moving Average (EMA) teacher encoder, $f_{\theta'}$, is used to generate stable targets. The student branch includes an encoder and a predictor head pred_{ψ} , which takes the student’s encoding of the masked context and attempts to map it to the teacher’s encoding of the target:

$$\mathcal{L}_{\text{JEPA}} = |\text{pred}_{\psi}(f_{\theta}(\mathbf{x}, \text{mask})) - f_{\theta'}(\mathbf{y})|_2^2 \quad (4)$$

To further regularize the latent space, a VicREG [3] loss is applied to the student embeddings.

Le-JEPA: We evaluate Le-JEPA [2], which replaces JEPA’s teacher-student architectures with a regularization-based approach to prevent representational collapse. This paradigm is built on the premise that an isotropic Gaussian represents the optimal embedding distribution for minimizing downstream prediction risk. To enforce this, Le-JEPA introduces Sketched Isotropic Gaussian Regularization (SIGReg), which constrains the latent space without requiring stop-gradients, EMA teachers, or heuristic schedulers. Specifically, the model minimizes the distance between the mean centroid of global view embeddings $\bar{\mathbf{z}}_g$ and augmented view embeddings \mathbf{z}_a . This similarity term is balanced with the SIGReg loss, which projects embeddings onto random unit vectors and applies a 1-D goodness-of-fit test T to enforce isotropy:

$$\mathcal{L}_{\text{Le-JEPA}} = (1 - \lambda) \cdot \underbrace{|\bar{\mathbf{z}}_g - \mathbf{z}_a|_2^2}_{\text{invariance}} + \lambda \cdot \underbrace{T(\mathbf{z}_m)}_{\text{SIGReg}} \quad (5)$$

where λ controls the trade-off between view invariance and latent distribution matching.

DINO: We evaluate the invariance-based DINO paradigm [4], originally popularized in computer vision. DINO employs a self-distillation framework where a student network is trained to match the output of a teacher network. To prevent collapse, the teacher is an EMA version of the student, and its outputs are centered and sharpened. The model minimizes the cross-entropy between the teacher and student output distributions (p):

$$\mathcal{L}_{\text{DINO}} = - \sum p\theta'(\mathbf{x}_{\text{teacher}}) \log p\theta(\mathbf{x}_{\text{student}}) \quad (6)$$

Novel Adaptation of Le-JEPA and DINO for Time Series While DINO and Le-JEPA rely on augmentations to challenge the encoder, standard vision-based transforms like cropping often fail to respect the temporal dependencies of time series data. We propose a novel adaptation for these paradigms utilizing DWT-based augmentations to enforce frequency-domain invariance. Given a signal \mathbf{x} , we generate two views via a Daubechies wavelet decomposition at level l :

- **Teacher View:** A "clean" reference generated via soft-thresholding of wavelet coefficients. This preserves the structural approximation (low-frequency trend) while smoothing out high-frequency noise.

- Student View: A "hard" view where detail coefficients are subjected to additive high-frequency noise thresholding and a $p\%$ zero-out ratio is applied to the finest levels.

By filtering localized transients through wavelet-based perturbations, the objective forces the latent space to capture the stable spectral signatures of the system rather than high-frequency stochasticity. Appendix A.7 presents an ablation study comparing the impact of these temporal augmentations against traditional vision-like transformations.

4 Experimental Results

4.1 Experimental Setup

Pre-training Data Composition. We investigate three data regimes: (i) *Real-only*, using the Monash repository [9], which comprises of diverse, real-world time series data (~680K samples); (ii) *Synthetic-only*, a 2.5M-sample corpus generated via the structural-prior framework of TimePFN [16], where time series are sampled from kernel-composition Gaussian Process priors and extended to multivariate settings via linear coregionalization (see Appendix A.8.1 for details); and (iii) *Hybrid*, a mixture of Monash and synthetic samples, with a total of 2.5M samples.

Evaluation and Downstream Tasks We assess representation quality through two distinct protocols: (i) *Linear Probing*, and (ii) *Full Fine-tuning*. In Linear Probing, the pre-trained backbone weights are frozen, and only a single linear layer is trained for the downstream task. This approach ensures that performance reflects the intrinsic quality and linear separability of the learned features, rather than the ability of a deep decoder to compensate for suboptimal representations. Conversely, Full Fine-tuning allows all model parameters to be updated, evaluating the backbone’s capacity for deep specialization. In both regimes, we quantify the value added by SSL by benchmarking against a randomly initialized backbone that undergoes the same task-specific training *without pre-training*. For all Linear Probing experiments, we report the mean and standard deviation across five random seeds to ensure statistical stability.

Our evaluation includes a diverse suite of time-series benchmarks spanning varying temporal dynamics and scales, and covering three task families: (i) *Forecasting*, performing multivariate sequence prediction on the ETT, Weather, Electricity, and Traffic datasets; (ii) *Classification*, covering nine heterogeneous benchmarks spanning gesture recognition, medical signals, and speech; and (iii) *Anomaly Detection*, involving point-wise detection in satellite telemetry and industrial systems. For all tasks, we follow the standard dataset splits and evaluation protocols of `tslib`[18], ensuring consistency with prior work.

Implementation and Training Details. To ensure a controlled comparison of SSL paradigms, we employ a Transformer backbone with the same architectural capacity and a patch size of 16. To investigate architectural scaling, we vary the number of layers $N \in \{2, 4, 8, 12, 24\}$. Pre-training is conducted for 20 epochs with a batch size of 128. Linear probing is conducted with task-specific optimization settings. All experiments were conducted on NVIDIA RTX PRO 6000 Blackwell GPUs (96GB VRAM), using a single GPU per run.

To support reproducibility, we provide extended details regarding the pre-training corpus, downstream benchmarks, evaluation protocols, augmentation strategy, implementation and training hyperparameters as well as compute resources, runtime, and memory usage, in Appendix A.8.

4.2 Evaluating Representation Quality with Linear Probing

We evaluate the representation quality of Generative and Latent Alignment SSL paradigms by pre-training an 8-layer Transformer on the Monash repository, followed by Linear Probing. We report the results obtained when pretraining on the synthetic and mix datasets in Appendices A.1-A.3

4.3 Time Series Anomaly Detection

Table 1 shows that the optimal pre-training paradigm depends on the specific nature of the benchmark. Latent Alignment (JEPA and Le-JEPA) excels on spacecraft telemetry datasets (MSL and SMAP), where capturing global morphology is key. On MSL, Le-JEPA yields a 159% improvement over the

non-pretrained baseline. On SMAP, JEPA achieves a 375% gain over the baseline, outperforming all Generative methods by a margin of 35–53%. These gains are characterized by high statistical stability across seeds, contrasting with the higher variance observed in Generative paradigms. On high-entropy server logs (PSM and SMD), the advantage shifts to Generative (NTP) and Invariance-based (DINO) paradigms, which outperform JEPA-based models by roughly 15%. The SWaT benchmark remains an outlier where no pre-trained model improves upon the baseline.

Table 1: Linear probing F1 scores (Mean \pm Std) on anomaly detection benchmarks. Models are pre-trained on the Monash dataset; top results per dataset are highlighted in **bold**.

Paradigm	MSL	PSM	SMAP	SMD	SWaT
<i>No Pretraining</i>	0.22	0.46	0.08	0.50	0.12
<i>Generative</i>					
NTP	0.22 \pm .005	0.63\pm.096	0.20 \pm .007	0.63\pm.003	0.12\pm.001
MAE	0.28 \pm .006	0.47 \pm .094	0.25 \pm .011	0.61 \pm .007	0.12\pm.001
Diffusion	0.56 \pm .004	0.46 \pm .006	0.18 \pm .001	0.51 \pm .002	0.11 \pm .001
<i>Latent-Alignment</i>					
DINO	0.20 \pm .014	0.62 \pm .074	0.19 \pm .020	0.62 \pm .007	0.12\pm.001
JEPA	0.57 \pm .000	0.46 \pm .002	0.38\pm.001	0.52 \pm .002	0.03 \pm .000
Le-JEPA	0.57\pm.001	0.47 \pm .002	0.34 \pm .006	0.52 \pm .003	0.03 \pm .000

4.3.1 Time Series Classification

The results in Table 2 suggests a similar trend for Classification tasks, where performance aligns with the compatibility between the nature of the underlying signal and the SSL objective. Le-JEPA and MAE emerge as the most effective choices across the benchmark suite. Le-JEPA achieves the highest accuracy on five of the nine datasets, showing substantial improvements in tasks governed by global morphology and gestures such as *Handwriting* (0.19) and *UWave* (0.76), where it more than doubles the performance of the non-pretrained baseline. Conversely, MAE is more effective for signals characterized by rigid periodicity and local recurrence, producing the top results for *EthanolConcentration* (0.29), *Heartbeat* (0.73), and *JapaneseVowels* (0.93). While Le-JEPA excels on shape-related benchmarks, other latent alignment methods like JEPA and DINO often struggle to improve upon the baseline, indicating that specific latent-space regularization is a key factor for extracting discriminative features in classification. Statistical stability is generally high across paradigms, though Generative methods exhibit higher variance on specific benchmarks like *SpokenArabicDigits* and *UWave* compared to the more stable performance of Le-JEPA.

Table 2: Linear probing accuracy (Mean \pm Std) on classification benchmarks. Datasets: **Eth** (Ethanol-Concentration), **Face** (FaceDetection), **Hand** (Handwriting), **Hrt** (Heartbeat), **Vwl** (JapaneseVowels), **S1/S2** (SCP1/S2), **Dig** (SpokenArabicDigits), **UW** (UWave). Models are pre-trained on the Monash dataset; top results per dataset are highlighted in **bold**.

Paradigm	Eth	Face	Hand	Hrt	Vwl	S1	S2	Dig	UW
<i>No Pretraining</i>	0.27	0.54	0.06	0.69	0.92	0.80	0.52	0.78	0.34
<i>Generative</i>									
NTP	0.27 \pm .011	0.55 \pm .003	0.06 \pm .013	0.71 \pm .026	0.93 \pm .011	0.75 \pm .017	0.52 \pm .024	0.89 \pm .004	0.55 \pm .028
MAE	0.29\pm.008	0.58 \pm .012	0.06 \pm .012	0.73\pm.024	0.93\pm.015	0.74 \pm .026	0.49 \pm .015	0.89 \pm .014	0.40 \pm .037
Diff.	0.25 \pm .012	0.55 \pm .020	0.06 \pm .027	0.67 \pm .025	0.88 \pm .059	0.67 \pm .037	0.54 \pm .024	0.81 \pm .049	0.49 \pm .019
<i>Latent Alignment</i>									
DINO	0.26 \pm .009	0.52 \pm .005	0.10 \pm .009	0.72 \pm .004	0.76 \pm .009	0.72 \pm .014	0.56\pm.010	0.70 \pm .011	0.42 \pm .059
JEPA	0.25 \pm .002	0.52 \pm .007	0.08 \pm .007	0.62 \pm .028	0.92 \pm .012	0.70 \pm .010	0.53 \pm .020	0.83 \pm .004	0.46 \pm .004
Le-JEPA	0.24 \pm .005	0.60\pm.004	0.19\pm.012	0.61 \pm .014	0.89 \pm .013	0.84\pm.023	0.49 \pm .017	0.93\pm.007	0.76\pm.006

4.3.2 Time Series Forecasting

Table 3 shows that the pre-training dividend for forecasting is marginal (typically 1%–3%), with the non-pretrained baseline remaining highly competitive and frequently matching or exceeding SSL performance across paradigms. While Generative models (Diffusion) and Latent Alignment (JEPA)

achieve isolated best results on specific datasets, the margins remain thin. Notably, Le-JEPA exhibits severe degradation across all benchmarks (e.g., an 83% MSE increase on *Traffic*). We further note that SSL benefit remains stable across horizons (detailed results shown in Appendix A.3)

Table 3: Linear probing performance (MSE) on forecasting benchmarks (Mean \pm Std). Datasets: **H1/H2** (ETTh1/2), **M1/M2** (ETTm1/2), **Wtr** (Weather), **Elec** (Electricity), **Trf** (Traffic). Lower is better; best results are **bolded**.

Paradigm	H1	H2	M1	M2	Wtr	Elec	Trf
<i>No Pretraining</i>	0.413	0.344	0.356	0.260	0.247	0.172	0.434
<i>Generative</i>							
NTP	0.437 \pm .002	0.362 \pm .001	0.352\pm.000	0.263 \pm .001	0.235 \pm .001	0.179 \pm .001	0.443 \pm .002
MAE	0.437 \pm .002	0.366 \pm .002	0.362 \pm .002	0.262 \pm .001	0.243 \pm .001	0.199 \pm .014	0.476 \pm .003
Diff.	0.425 \pm .002	0.334\pm.001	0.360 \pm .002	0.262 \pm .001	0.238 \pm .001	0.193 \pm .003	0.466 \pm .006
<i>Latent Alignment</i>							
DINO	0.431 \pm .003	0.359 \pm .003	0.358 \pm .002	0.252\pm.001	0.236 \pm .001	0.179 \pm .005	0.439 \pm .008
JEPA	0.441 \pm .001	0.384 \pm .001	0.359 \pm .001	0.274 \pm .001	0.233\pm.000	0.170\pm.000	0.425\pm.003
Le-JEPA	0.591 \pm .014	0.404 \pm .005	0.406 \pm .006	0.280 \pm .002	0.248 \pm .001	0.304 \pm .018	0.795 \pm .048

4.4 Full Fine-Tuning Performance

To evaluate the capacity for deep specialization, we compare the average performance of different SSL paradigms when the entire backbone is fine-tuned (Table 4). Latent Alignment provides a more effective initialization than Generative paradigms. While DINO struggles in Classification under the Linear Probing regime, it achieves the highest average accuracy (0.65) with Full Fine-Tuning. This suggests that while invariance-based pre-training may not immediately yield linearly separable features, it establishes a superior weight initialization for semantic tasks. For Anomaly Detection, JEPA achieves the strongest overall results (0.39), outperforming both Generative methods and the non-pretrained baseline. On Forecasting, however, we find that the baseline remains highly competitive, outperforming all other methods and matching the 0.29 MSE achieved by JEPA. We further provide the detailed full results for each dataset in Appendix A.4.

Table 4: Summary of Full Fine-tuning performance across all tasks. Results are averaged across all datasets per task. Top results per task are highlighted in **bold**.

Paradigm	Anomaly (F1) \uparrow	Class. (Acc) \uparrow	Forecasting (MSE) \downarrow
<i>No Pretraining (Baseline)</i>	0.3011	0.5451	0.2963
<i>Generative</i>			
NTP	0.2738	0.5894	0.3339
MAE	0.2890	0.5433	0.3494
Diff	0.3836	0.5915	0.3404
<i>Latent Alignment</i>			
DINO	0.2648	0.6477	0.3304
JEPA	0.3891	0.5324	0.2935
Le-JEPA	0.3766	0.6077	0.3873

In addition to Linear Probing and Full Fine-tuning, we also applied an "intermediate" evaluation protocol, where an MLP head is trained on top of a frozen backbone. The results of this experiment, provided in Appendix A.5, show consistent trends with our linear evaluation.

4.5 Scaling and Data Composition Analysis

To understand the factors driving representation quality beyond the choice of SSL objective, we investigate how performance relates to data composition and model capacity.

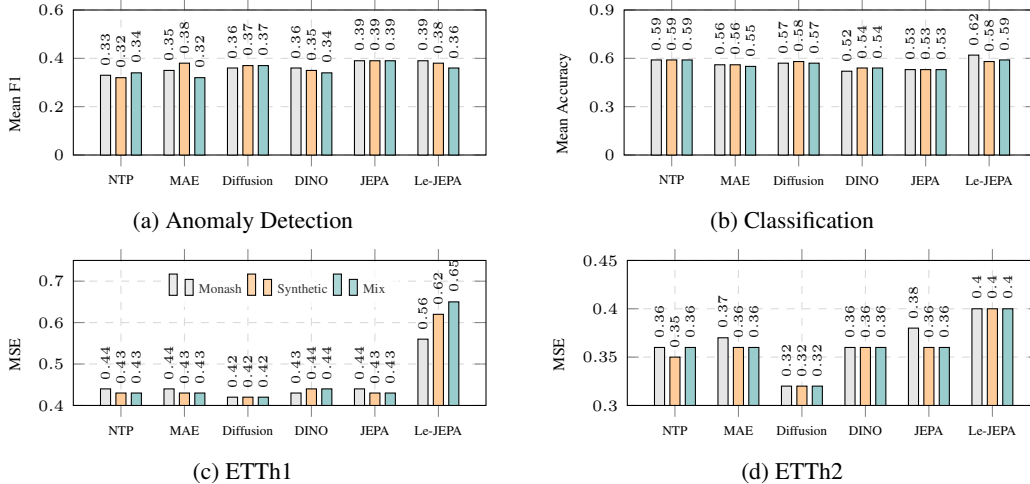


Figure 1: Impact of pre-training data composition.

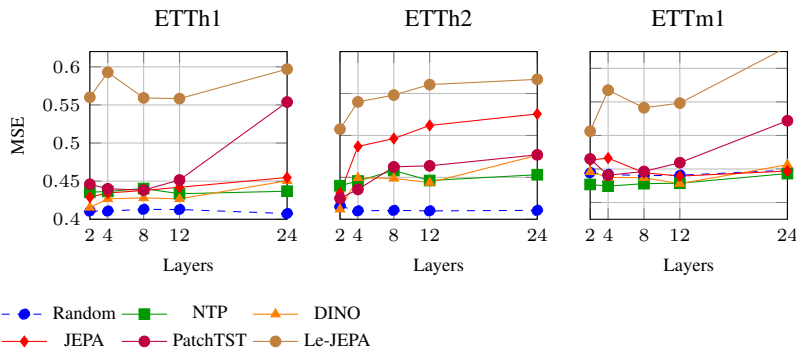


Figure 2: Forecasting performance (MSE) as a function of backbone depth.

4.5.1 Impact of Data Source and Composition

The influence of pre-training data composition reveals a notable indifference to data origin in most tasks (Figure 1). For both anomaly detection and forecasting, there is almost no performance difference between data regimes; in fact, synthetic pre-training occasionally yields better results. This finding is surprising given that the Monash repository contains datasets that directly overlap with some of our downstream benchmarks (e.g., weather and electricity). This suggests that these SSL paradigms can scale effectively using massive synthetic datasets without relying on limited or domain-specific real-world observations. In classification, the choice of data source mainly affects Le-JEPA, where pre-training on real-world signals leads to an increase in accuracy from 0.58 to 0.62. For the remaining paradigms, the differences between real and synthetic data remain marginal, reinforcing the potential of using large-scale synthetic datasets as surrogates for real-world data.

4.5.2 Impact of Architectural Depth

Figure 2 illustrates forecasting performance relative to Transformer depth (number of layers N). Across most paradigms, performance typically saturates between 8 and 12 layers, with diminishing returns or slight degradation observed at $N = 24$. While deeper architectures generally offer smoother convergence, the relative performance ranking of SSL paradigms remains consistent across scales. These results suggest that the utility of pre-training for forecasting is primarily determined by the qualitative nature of the learned representations rather than raw architectural capacity.

5 Lessons Learned

In light of the experimental results, we revisit our primary research questions.

RQ1. What is the added value of SSL across diverse time series task families? The "dividend" of pre-training is highly asymmetric across task families. In anomaly detection, pre-training provides a massive dividend, yielding up to a 375% improvement, by establishing a robust representational baseline for "normal" signal behavior. In classification, the gain is similarly substantial but remains conditional on the SSL objective aligning with the underlying signal morphology. Importantly, these trends persist under full fine-tuning, where pre-trained initializations consistently outperform randomly initialized counterparts for semantic tasks.

Conversely, in forecasting, the dividend remains marginal (1%–3%) or even negative across all paradigms. The strong performance of the randomly initialized baseline suggests that for sequence prediction, the architectural inductive biases of the backbone (e.g., temporal patching) are the primary drivers of performance, largely overshadowing the benefits of specialized SSL pre-training in the linear probing and fine-tuning regimes.

RQ2. How does the choice of SSL objective dictate downstream performance? The utility of SSL representations is not universal; its transferability is governed by whether the pre-training objective preserves the specific signal resolution required by the downstream task. We find that Latent Alignment paradigms (JEPA, DINO, LeJEPA) prioritize global structural characteristics, though their utility is highly sensitive to the evaluation regime. In Classification, a performance divergence emerges: while DINO and JEPA struggle under constrained Linear Probing, LeJEPA excels by utilizing Sketched Isotropic Gaussian Regularization (SIGReg) to enforce latent isotropy, maximizing linear separability. However, under Full Fine-Tuning, DINO emerges as the superior approach, suggesting that invariance-based pre-training builds a more adaptable, albeit not immediately separable, semantic representation. In Anomaly Detection, the advantage is task-dependent. LeJEPA and JEPA’s predictive latent alignment prove most effective for capturing the global morphology of system failures (e.g., spacecraft telemetry), while Generative paradigms (NTP, MAE) preserve the high-resolution local dynamics necessary for granular server-log anomaly detection, outperforming Latent Alignment by $\sim 15\%$ in those settings. Despite its strength in semantic tasks, LeJEPA fails severely in forecasting. We hypothesize that the combination of view invariance and SIGReg, which forces embeddings toward an isotropic distribution, effectively filters out the low-variance, point-wise temporal dependencies required for accurate sequence prediction. This focus on semantic abstraction comes at the cost of the local detail preserved by Generative models. This fundamental "precision vs. invariance" trade-off suggests that a hybrid multi-objective paradigm may be necessary to unlock the potential of universal time series foundation models.

RQ3. To what extent is representation quality driven by data origin and architectural scale? A key insight from our study is the high utility of synthetic data in pre-training. For anomaly detection and forecasting, performance remains largely independent of data origin; pre-training on general synthetic datasets often matches the results of real-world data, even when the latter contains domain-specific overlap with the downstream task. This suggests that the scaling of time-series SSL may be more effectively navigated through massive-scale synthetic generation rather than exhaustive real-world collection. Furthermore, the performance saturation observed at 8–12 layers across all paradigms indicates that current SSL utility is not limited by model capacity under the investigated regimes. Instead, these models appear to be bottlenecked by data scaling and the qualitative nature of the SSL objectives, suggesting that simply increasing model parameters may yield diminishing returns without fundamental innovations in objective design.

6 Conclusion

Summary. We provide a systematic evaluation of generative and latent temporal SSL, including novel adaptations of DINO and LeJEPA for time series. Our results demonstrate that the "pre-training dividend" is highly asymmetric and governed by a precision-invariance trade-off, where representational utility depends on the signal resolution required by the task. Finally, we show that data scale overshadows origin, with synthetic pre-training achieving parity with real-world data.

Limitations and Future Work. This study focuses exclusively on Transformer-based backbones; future research should investigate if these trade-offs persist in alternative architectures such as Convolutional and State-Space Models. Additionally, while we identify a performance bottleneck in current objectives, the design of hybrid paradigms, advanced time series augmentations for latent alignment methods and training on massive synthetic datasets remain directions for future research.

References

- [1] Abdul Fatir Ansari, Lorenzo Stella, Caner Turkmen, Xiyuan Zhang, Pedro Mercado, Huibin Shen, Oleksandr Shchur, Syama Sundar Rangapuram, Sebastian Pineda Arango, Shubham Kapoor, et al. Chronos: Learning the language of time series. *arXiv preprint arXiv:2403.07815*, 2024.
- [2] Randall Balestriero and Yann LeCun. Lejepa: Provable and scalable self-supervised learning without the heuristics, 2025. URL <https://arxiv.org/abs/2511.08544>, 10.
- [3] Adrien Bardes, Jean Ponce, and Yann LeCun. VICReg: Variance-invariance-covariance regularization for self-supervised learning. In *International Conference on Learning Representations*, 2022.
- [4] Mathilde Caron, Hugo Touvron, Ishan Misra, Hervé Jégou, Julien Mairal, Piotr Bojanowski, and Armand Joulin. Emerging properties in self-supervised vision transformers. In *International Conference on Computer Vision (ICCV)*, 2021.
- [5] Abhimanyu Das, Weihao Kong, Rajat Sen, and Yichen Zhou. A decoder-only foundation model for time-series forecasting. *arXiv preprint arXiv:2310.10688*, 2023.
- [6] Qingsong Dong, Yuxuan Ma, Yu Wang, Jie Chen, and Jun Wang. Simmtm: A simple pre-training framework for masked time-series modeling. In *Advances in Neural Information Processing Systems (NeurIPS)*, 2023.
- [7] Qingsong Dong, Yuxuan Ma, Yu Wang, Jie Chen, and Jun Wang. Timesiam: Siamese self-supervised learning for time series. In *International Conference on Machine Learning (ICML)*, 2024.
- [8] Sofiane Ennadir, Siavash Golkar, and Leopoldo Sarra. Joint embeddings go temporal. *arXiv preprint arXiv:2509.25449*, 2025.
- [9] Rakshitha Godahewa, Christoph Bergmeir, Geoffrey I Webb, Rob J Hyndman, and Pablo Montero-Manso. Monash time series forecasting archive. *arXiv preprint arXiv:2105.06643*, 2021.
- [10] Yann LeCun. Joint embedding predictive architectures: Self-supervised learning without reconstruction. *arXiv preprint arXiv:2301.08243*, 2023.
- [11] Ziyu Liu, Azadeh Alavi, Minyi Li, and Xiang Zhang. Self-supervised learning for time series: Contrastive or generative? *arXiv preprint arXiv:2403.09809*, 2024.
- [12] Yessin Moakher, Youssef Attia El Hili, and Vasiliï Feofanov. Utica: Multi-objective self-distillation foundation model pretraining for time series classification. *arXiv preprint arXiv:2603.01348*, 2026.
- [13] Yuqi Nie, Nam H Nguyen, Phanwadee Sinthong, and Jayant Kalagnanam. A time series is worth 64 words: Long-term forecasting with transformers. *arXiv preprint arXiv:2211.14730*, 2022.
- [14] Yuqi Nie, Nam H Nguyen, Phanwadee Sinthong, and Jayant Kalagnanam. A time series is worth 64 words: Long-term forecasting with transformers. *arXiv preprint arXiv:2211.14730*, 2022.
- [15] Aaron van den Oord, Yazhe Li, and Oriol Vinyals. Representation learning with contrastive predictive coding. In *arXiv preprint arXiv:1807.03748*, 2018.
- [16] Ege Onur Taga, Muhammed Emrullah Ildiz, and Samet Oymak. Timepfn: Effective multivariate time series forecasting with synthetic data. In *Proceedings of the AAAI conference on artificial intelligence*, volume 39, pages 20761–20769, 2025.
- [17] Ashish Vaswani, Noam Shazeer, Niki Parmar, Jakob Uszkoreit, Llion Jones, Aidan N Gomez, Łukasz Kaiser, and Illia Polosukhin. Attention is all you need. *Advances in neural information processing systems*, 30, 2017.

- [18] Yuxuan Wang, Haixu Wu, Jiayang Dong, Yong Liu, Chen Wang, Mingsheng Long, and Jianmin Wang. Deep time series models: A comprehensive survey and benchmark. *arXiv preprint arXiv:2407.13278*, 2024.
- [19] Zhihan Yue, Haoyue Liu, Yan Zhou, Huan Yu, and Wenwu Sun. Ts2vec: Towards universal representation of time series. In *AAAI Conference on Artificial Intelligence*, 2022.
- [20] George Zerveas, S Jayaraman, Dhaval Patel, Anurag Bhamidipaty, and Carsten Eickhoff. Self-supervised learning for time series analysis: Taxonomy, progress, and prospects. *IEEE Transactions on Pattern Analysis and Machine Intelligence*, 2023.
- [21] Qingsong Zhang et al. Timedart: Diffusion-based autoregressive representation learning for time series. *arXiv preprint arXiv:2410.05711*, 2024.
- [22] Qingsong Zhang et al. Universal time-series representation learning: A survey. *arXiv preprint arXiv:2401.03717*, 2024.

A Appendix

We provide extended results and discussion that did not fit within the page limitation of the main text and a detailed documentation of our experimental setup to support reproducibility:

- Sections A.1- A.3 provide extended Linear Probing evaluation results for Anomaly Detection, Classification and Forecasting, respectively, under different pre-training data regimes. For Forecasting we report the detailed results per horizon.
- Section A.4 reports extended results for our Full Fine-tuning evaluation.
- Section A.5 includes additional results under an MLP-based probing evaluation protocol. In this setting, an MLP head is trained on top of a frozen backbone.
- Section A.6 shows a qualitative analysis of learned embedding through t-SNE visualization.
- Section A.7 provides the results of an ablation study of the proposed augmentations for DINO and LeJEPA.
- Section A.8 gives extended details of our experimental setup, encompassing:
 - Pretraining datasets details (Appendix A.8.1)
 - Additional details on our evaluation benchmarks and metrics (Appendix A.8.2)
 - Hyper-parameter and detailed specification for our implementation and training (Appendix A.8.3)
 - Compute and train time details (Appendix A.8.4)
- Section A.9 provides results for a converge analysis to evaluate our choice of pretraining "budget".
- Section A.10 gives additional analysis and implementation details for LeJEPA and DINO, to further evaluate their behavior under the proposed adaptation.

A.1 Extended Anomaly Detection Results (Linear Probing)

Tables 1, 5, and 6 provide the full anomaly detection results under the Synthetic, and Mixed pre-training, respectively (the results for the Monash dataset are provided in the main text). Overall, the results confirm that anomaly detection benefits more clearly from SSL than forecasting, but the optimal paradigm depends strongly on the anomaly type and dataset domain.

Across all data regimes, latent-alignment methods are strongest on spacecraft telemetry datasets. JEPA and Le-JEPA consistently achieve the best or near-best results on MSL and SMAP, substantially improving over the non-pretrained baseline. This suggests that these datasets benefit from representations that capture global system-state morphology and deviations from expected temporal structure. In contrast, high-dimensional service-monitoring datasets such as PSM and SMD favor target-domain restoration methods and DINO. NTP achieves the strongest results on SMD under Synthetic and Mixed pre-training, while DINO and NTP are highly competitive on PSM, indicating that local reconstruction and structured invariance are better aligned with noisy operational signals.

The effect of pre-training data composition is meaningful but not uniform. Synthetic and Mixed pre-training improve some restoration-based results, especially NTP on PSM and SMD, but do not consistently improve latent-alignment methods. JEPA and Le-JEPA remain stable on MSL and SMAP across data regimes, whereas their performance remains weak on SWaT. SWaT is a consistent outlier: the non-pretrained baseline is competitive or best across all regimes, suggesting that the SSL objectives considered here do not capture the physical-control constraints that characterize this dataset.

Taken together, these results reinforce the main conclusion that SSL utility in anomaly detection is task- and domain-dependent. Latent-alignment objectives are effective when anomalies correspond to global system-state changes, while restoration-based objectives are more effective for noisy, high-dimensional monitoring data. Data composition can shift the relative ranking, but it does not produce a universally superior pre-training regime.

Table 5: Anomaly detection performance (F1 scores) after pre-training on a large synthetic corpus. Top results are highlighted in **bold**.

SSL Paradigm	MSL	PSM	SMAP	SMD	SWaT
<i>No Pre-training</i>	0.2225	0.4643	0.0783	0.4971	0.1180
<i>Generative</i>					
NTP	0.2001	0.5353	0.1445	0.6154	0.1169
MAE	0.2890	0.6300	0.2432	0.6149	0.1179
Diffusion	0.5666	0.4105	0.2927	0.5105	0.0639
<i>Latent Alignment</i>					
DINO	0.2167	0.6320	0.1571	0.6136	0.1168
JEPA	0.5683	0.4355	0.3821	0.5238	0.0291
Le-JEPA	0.5690	0.4156	0.3378	0.5235	0.0292

Table 6: Anomaly detection performance (F1 scores) after pre-training on a hybrid mixture of real-world (Monash) and synthetic data. Top results are highlighted in **bold**.

SSL Paradigm	MSL	PSM	SMAP	SMD	SWaT
<i>No Pre-training</i>	0.2225	0.4643	0.0783	0.4971	0.1180
<i>Generative</i>					
NTP	0.1975	0.6117	0.1598	0.6266	0.1173
MAE	0.2922	0.3069	0.2694	0.6192	0.1179
Diffusion	0.5667	0.3923	0.3000	0.5136	0.0599
<i>Latent Alignment</i>					
DINO	0.2236	0.5554	0.1875	0.6261	0.1177
JEPA	0.5680	0.4483	0.3803	0.5237	0.0292
Le-JEPA	0.5678	0.3637	0.3359	0.5267	0.0287

A.2 Extended Classification Results (Linear Probing)

Tables 2, 7, and 8 report classification performance under the Synthetic, and Mixed pre-training regimes, respectively (the results for the Monash dataset are provided in the main text). Overall, SSL methods present substantial and consistent gains over the non-pretrained baseline on several datasets.

Across all data regimes, Le-JEPA emerges as one of the most effective methods on tasks governed by global morphology and structured temporal patterns. It consistently achieves top or near-top performance on datasets such as *Handwriting*, *FaceDetection*, *Digits*, and *UWave*, often with large margins over both the baseline and competing SSL paradigms. Notably, these gains are stable across pre-training regimes, indicating that the invariance and latent-structure constraints introduced by Le-JEPA capture robust, transferable representations for shape-driven classification tasks.

In contrast, target-domain restoration methods perform best on datasets characterized by strong periodicity and local temporal dependencies. This trend is consistent across all regimes, with MAE

achieving strong results on *Ethanol* and *Heartbeat*, while NTP is competitive and often achieves the best performance on *JapaneseVowels*.

The effect of data composition is present but secondary to the choice of SSL objective. Synthetic and Mixed pre-training slightly improve performance on certain datasets, particularly for restoration-based methods, but do not fundamentally alter the relative ranking between paradigms. Le-JEPA remains dominant on morphology-driven tasks across all regimes, while restoration-based methods (MAE and NTP) consistently lead on periodic signals.

Latent alignment methods without explicit invariance regularization (DINO, JEPA) show more variable behavior. While DINO performs competitively on certain datasets (e.g., SCP2 under Mixed pre-training), and JEPA achieves moderate improvements over the baseline, both methods frequently underperform relative to Le-JEPA. This highlights the importance of carefully designed invariance constraints for extracting discriminative features in classification tasks.

Finally, classification results exhibit relatively high statistical stability across paradigms, as reflected in Table 2. While generative methods show increased variance on datasets such as *Digits* and *UWave*, Le-JEPA maintains consistently low variance alongside strong performance, reinforcing its robustness.

Overall, these results demonstrate that while classification benefits substantially from SSL, the optimal paradigm is strongly tied to the underlying signal structure: invariance-driven alignment excels for shape-based discrimination, while reconstruction-based objectives are better suited for periodic and locally structured signals. Data composition plays a secondary role, refining performance but not fundamentally altering these trends.

Table 7: Linear probing accuracy on classification benchmarks after pre-training on a large synthetic corpus. Models are grouped by SSL paradigm; the top result for each dataset across all categories is highlighted in **bold**.

SSL Paradigm	Ethanol	FaceDet	Handwrit	Heartbt	JapVowel	SCP1	SCP2	Digits	UWave
<i>No Pre-training</i>	0.2662	0.5417	0.0624	0.6878	0.9243	0.7952	0.5222	0.7763	0.3438
<i>Generative</i>									
NTP	0.2738	0.5897	0.0541	0.7317	0.9649	0.7065	0.5333	0.8545	0.6156
MAE	0.3080	0.5525	0.0553	0.7805	0.8865	0.7235	0.5500	0.8222	0.3375
Diffusion	0.251	0.5707	0.0953	0.6537	0.9216	0.7474	0.5333	0.8836	0.5531
<i>Latent Alignment</i>									
DINO	0.2738	0.5210	0.0871	0.7220	0.7919	0.7167	0.5000	0.8072	0.4344
JEPA	0.2433	0.5224	0.0729	0.6098	0.9162	0.6246	0.5056	0.8126	0.4656
Le-JEPA	0.2243	0.5902	0.1694	0.6488	0.8216	0.7474	0.4222	0.9163	0.6969

Table 8: Linear probing accuracy on classification benchmarks after pre-training on a hybrid mixture of real-world (Monash) and synthetic data. Models are grouped by SSL paradigm; the top result for each dataset across all categories is highlighted in **bold**.

SSL Paradigm	Ethanol	FaceDet	Handwrit	Heartbt	JapVowel	SCP1	SCP2	Digits	UWave
<i>No Pre-training</i>	0.2662	0.5417	0.0624	0.6878	0.9243	0.7952	0.5222	0.7763	0.3438
<i>Generative</i>									
NTP	0.2890	0.5897	0.0694	0.7122	0.9514	0.7543	0.5222	0.8527	0.5563
MAE	0.2966	0.5423	0.0306	0.7415	0.9027	0.7679	0.4889	0.8076	0.3719
Diffusion	0.2433	0.5797	0.0871	0.6146	0.8946	0.7201	0.5500	0.8945	0.5719
<i>Latent Alignment</i>									
DINO	0.2738	0.5131	0.0941	0.7220	0.7784	0.7304	0.5444	0.7021	0.5125
JEPA	0.2433	0.5201	0.0718	0.6049	0.9162	0.6246	0.4944	0.8140	0.4594
Le-JEPA	0.2852	0.6138	0.1824	0.6098	0.8865	0.7065	0.4000	0.9341	0.7156

A.3 Extended Forecasting Results (Linear Probing)

Horizon-wise Analysis. Tables 9 and 10 report forecasting performance across prediction horizons. Across all datasets, error increases monotonically with the prediction horizon, reflecting the growing

Table 9: Linear probing MSE across prediction horizons using an 8-layer backbone pre-trained on the Monash dataset. Lower is better; best results per dataset and horizon are highlighted in **bold**.

SSL Paradigm	ETTh1			ETTh2			ETTm1					
	96	192	336	720	96	192	336	720	96	192	336	720
<i>No Pre-training</i>	0.374	0.409	0.425	0.444	0.278	0.342	0.363	0.394	0.295	0.334	0.371	0.424
<i>Generative</i>												
NTP	0.391	0.427	0.451	0.492	0.296	0.361	0.377	0.419	0.290	0.329	0.365	0.421
MAE	0.397	0.425	0.450	0.481	0.295	0.362	0.384	0.419	0.306	0.337	0.369	0.422
Diffusion	0.383	0.415	0.413	0.459	0.266	0.316	0.307	0.381	0.306	0.342	0.376	0.427
<i>Latent Alignment</i>												
DINO	0.387	0.423	0.443	0.459	0.287	0.355	0.382	0.414	0.297	0.333	0.370	0.426
JEPA	0.398	0.439	0.455	0.459	0.323	0.388	0.390	0.413	0.298	0.336	0.372	0.425
Le-JEPA	0.520	0.556	0.572	0.589	0.333	0.399	0.409	0.456	0.342	0.376	0.407	0.461

Table 10: Linear probing MSE across prediction horizons using an 8-layer backbone pre-trained on the Monash dataset. Lower is better; best results per dataset and horizon are highlighted in **bold**.

SSL Paradigm	ETTm2				Weather				Electricity				Traffic			
	96	192	336	720	96	192	336	720	96	192	336	720	96	192	336	720
<i>No Pre-training</i>	0.167	0.223	0.280	0.370	0.175	0.217	0.264	0.333	0.144	0.158	0.174	0.212	0.411	0.424	0.436	0.464
<i>Generative</i>																
NTP	0.167	0.225	0.280	0.371	0.159	0.203	0.253	0.324	0.150	0.165	0.181	0.219	0.420	0.435	0.448	0.473
MAE	0.171	0.228	0.282	0.379	0.169	0.212	0.261	0.332	0.170	0.182	0.195	0.230	0.447	0.462	0.471	0.495
Diffusion	0.169	0.226	0.285	0.372	0.164	0.209	0.258	0.324	0.16	0.174	0.193	0.231	0.436	0.453	0.468	0.497
<i>Latent Alignment</i>																
DINO	0.163	0.219	0.270	0.359	0.159	0.203	0.253	0.325	0.147	0.162	0.179	0.219	0.411	0.425	0.438	0.466
JEPA	0.176	0.239	0.295	0.383	0.158	0.202	0.251	0.323	0.143	0.157	0.174	0.210	0.402	0.416	0.429	0.455
Le-JEPA	0.188	0.245	0.296	0.378	0.174	0.216	0.264	0.334	0.265	0.276	0.292	0.328	0.716	0.728	0.748	0.772

difficulty of long-range forecasting. However, consistent with our main findings, we do not observe systematic gains from SSL as the horizon increases.

The relative ranking between methods remains largely stable across horizons, but varies across datasets. On ETTh1 the *No Pre-training* baseline consistently outperforms or matches all pre-trained models across all horizons, indicating limited benefit from SSL in these settings. On ETTm1, *Generative* methods (in particular NTP) achieve the best performance across all horizons, although the margin over other methods remains small and does not increase with prediction length.

In contrast, other datasets exhibit clearer but still modest benefits from SSL. On ETTm2, *Latent Alignment* (DINO) consistently achieves the best performance across all horizons. On Weather and Electricity, both *Latent Alignment* (JEPA) and *Generative* methods (NTP) are competitive, with JEPA achieving the best results on most horizons. Importantly, these advantages remain stable across horizons rather than increasing with prediction length.

Overall, these results reinforce that improvements from SSL are primarily dataset-dependent and modest in magnitude. The absence of increasing gains at longer horizons suggests that current SSL objectives do not fundamentally enhance the modeling of long-term temporal dependencies, but instead provide task-specific inductive biases that are beneficial only under certain data characteristics.

Impact of Pre-training Data Composition. Figures 3–6 and Tables 11–13 report the effect of pre-training data composition on forecasting performance across datasets. Overall, the effect of data source is dataset-dependent and generally modest.

For ETTh1 and ETTh2, Synthetic and Mix pre-training often provide slight improvements over Monash for several methods, although the relative differences remain small. Within the *Generative* paradigm, Diffusion is particularly strong on ETTh2, while *Latent Alignment* (Le-JEPA) consistently underperforms on ETTh1.

Table 11: Linear probing performance on forecasting benchmarks using an 8-layer backbone pre-trained on the **Monash** dataset. Results are averaged across prediction horizons {96, 192, 336, 720}. Lower is better; best results per dataset are highlighted in **bold**.

SSL Paradigm	ETTh1		ETTh2		ETTm1		ETTm2		Weather		Electricity		Traffic	
	MAE	MSE	MAE	MSE	MAE	MSE	MAE	MSE	MAE	MSE	MAE	MSE	MAE	MSE
<i>No Pre-training</i>	0.4250	0.4130	0.3883	0.3443	0.3793	0.3560	0.3175	0.2600	0.2810	0.2473	0.2668	0.1720	0.2963	0.4335
<i>Generative</i>														
NTP	0.4430	0.4403	0.3990	0.3633	0.3808	0.3513	0.3190	0.2608	0.2695	0.2348	0.2770	0.1793	0.3108	0.4440
MAE	0.4363	0.4383	0.4010	0.3650	0.3870	0.3593	0.3258	0.2650	0.2795	0.2435	0.2965	0.1945	0.3373	0.4683
Diffusion	0.4358	0.4175	0.3738	0.3175	0.3843	0.3583	0.3180	0.2615	0.2710	0.2353	0.2890	0.1875	0.3333	0.4598
<i>Latent Alignment</i>														
DINO	0.4400	0.4280	0.4008	0.3595	0.3843	0.3548	0.3105	0.2538	0.2710	0.2350	0.2725	0.1760	0.2998	0.4335
JEPA	0.4358	0.4378	0.4163	0.3785	0.3840	0.3578	0.3300	0.2733	0.2673	0.2335	0.2648	0.1710	0.2955	0.4255
Le-JEPA	0.5160	0.5617	0.4253	0.3993	0.4155	0.3965	0.3353	0.2768	0.2823	0.2470	0.3835	0.2903	0.4893	0.7410

Table 12: Linear probing performance on forecasting benchmarks using an 8-layer backbone pre-trained on the **Synthetic** dataset. Results are averaged across prediction horizons {96, 192, 336, 720}. Lower is better; best results per dataset are highlighted in **bold**.

SSL Paradigm	ETTh1		ETTh2		ETTm1		ETTm2		Weather		Electricity		Traffic	
	MAE	MSE	MAE	MSE	MAE	MSE	MAE	MSE	MAE	MSE	MAE	MSE	MAE	MSE
<i>No Pre-training</i>	0.4250	0.4130	0.3883	0.3443	0.3788	0.3568	0.3148	0.2568	0.2795	0.2460	0.2645	0.1705	0.2963	0.4338
<i>Generative</i>														
NTP	0.4353	0.4293	0.3950	0.3535	0.3790	0.3503	0.3165	0.2578	0.2698	0.2355	0.2670	0.1718	0.2975	0.4318
MAE	0.4425	0.4313	0.3973	0.3633	0.3900	0.3678	0.3195	0.2620	0.2788	0.2435	0.2850	0.1870	0.3303	0.4615
Diffusion	0.4340	0.4205	0.3765	0.3243	0.3845	0.3608	0.3215	0.2650	0.2718	0.2358	0.2880	0.1848	0.3290	0.4578
<i>Latent Alignment</i>														
DINO	0.4458	0.4383	0.4008	0.3620	0.3835	0.3573	0.3113	0.2530	0.2720	0.2353	0.2775	0.1783	0.3060	0.4393
JEPA	0.4300	0.4288	0.3980	0.3583	0.3823	0.3625	0.3233	0.2660	0.2713	0.2378	0.2625	0.1690	0.2968	0.4300
Le-JEPA	0.5405	0.6163	0.4250	0.4005	0.4330	0.4243	0.3353	0.2763	0.2870	0.2513	0.3935	0.3000	0.5050	0.7665

On the ETTm datasets, the ranking between methods remains largely stable across data regimes. On ETTm1, *Generative* methods (NTP) are consistently among the strongest performers, while on ETTm2, *Latent Alignment* (DINO) achieves the best results across all regimes, with only minor variation between Monash, Synthetic, and Mix pre-training.

Weather and Electricity exhibit similarly limited sensitivity to data composition. On these datasets, *Latent Alignment* (JEPA) and *Generative* methods (NTP) are generally competitive, while Le-JEPA consistently underperforms, particularly on Electricity.

Traffic exhibits the largest sensitivity to data composition. In particular, Le-JEPA degrades substantially under Synthetic and Mix pre-training, while both *Generative* (NTP) and *Latent Alignment* (JEPA) perform better under Monash pre-training than under Synthetic or Mix.

Overall, these results reinforce that data composition alone does not provide a uniform improvement in forecasting performance. Instead, its effect depends strongly on the interaction between dataset characteristics and the SSL objective, with no single pre-training regime consistently dominating across benchmarks.

A.4 Extended Results for Full Fine-tuning Evaluation

We evaluate the effectiveness of SSL pre-training under full fine-tuning, where all model parameters are updated for the downstream task. Table 4 in the main text summarizes the average performance across tasks, while Tables 14, 15, and 16 provide detailed per-dataset results.

Overall Trends. Across tasks, *Latent Alignment* methods provide the strongest overall initialization under full fine-tuning. In particular, DINO achieves the highest average classification accuracy (0.65), while JEPA achieves the best anomaly detection performance (0.39). In contrast, *Generative* methods show more moderate improvements and remain less consistent across tasks. Notably, forecasting remains largely unaffected by pre-training, with the *No Pre-training* baseline remaining competitive and achieving the best or near-best performance across datasets.

Anomaly Detection. Table 14 shows that full fine-tuning amplifies the advantages of *Latent Alignment* methods on structured anomaly detection benchmarks. JEPA and Le-JEPA achieve the best results on MSL (0.57), substantially outperforming both the baseline (0.49) and *Generative*

Table 13: Linear probing performance on forecasting benchmarks using an 8-layer backbone pre-trained on the **hybrid mixture of real-world (Monash) and synthetic data** dataset. Results are averaged across prediction horizons {96, 192, 336, 720}. Lower is better; best results per dataset are highlighted in **bold**.

SSL Paradigm	ETTh1		ETTh2		ETTh1		ETTh2		Weather		Electricity		Traffic	
	MAE	MSE	MAE	MSE	MAE	MSE	MAE	MSE	MAE	MSE	MAE	MSE	MAE	MSE
<i>No Pre-training</i>	0.4250	0.4130	0.3883	0.3443	0.3788	0.3568	0.3148	0.2568	0.2795	0.2460	0.2645	0.1705	0.2963	0.4338
<i>Generative</i>														
NTP	0.4347	0.4297	0.3955	0.3557	0.379	0.3492	0.3167	0.2597	0.269	0.235	0.2672	0.172	0.298	0.4325
MAE	0.437	0.4297	0.3977	0.3627	0.39	0.3642	0.3212	0.262	0.273	0.2385	0.28175	0.1837	0.32625	0.45925
Diffusion	0.4415	0.423	0.376	0.32175	0.3907	0.3637	0.3177	0.2602	0.2747	0.238	0.318	0.2087	0.3667	0.4977
<i>Latent Alignment</i>														
DINO	0.4447	0.4365	0.4022	0.3625	0.3822	0.3557	0.311	0.2532	0.272	0.2357	0.2792	0.18	0.3095	0.443
JEPA	0.431	0.4287	0.4017	0.3635	0.3835	0.3635	0.3237	0.2677	0.273	0.2385	0.2627	0.169	0.297	0.4292
Le-JEPA	0.5495	0.6457	0.4275	0.4025	0.4462	0.4487	0.3435	0.2842	0.2915	0.255	0.4087	0.3185	0.52725	0.8127

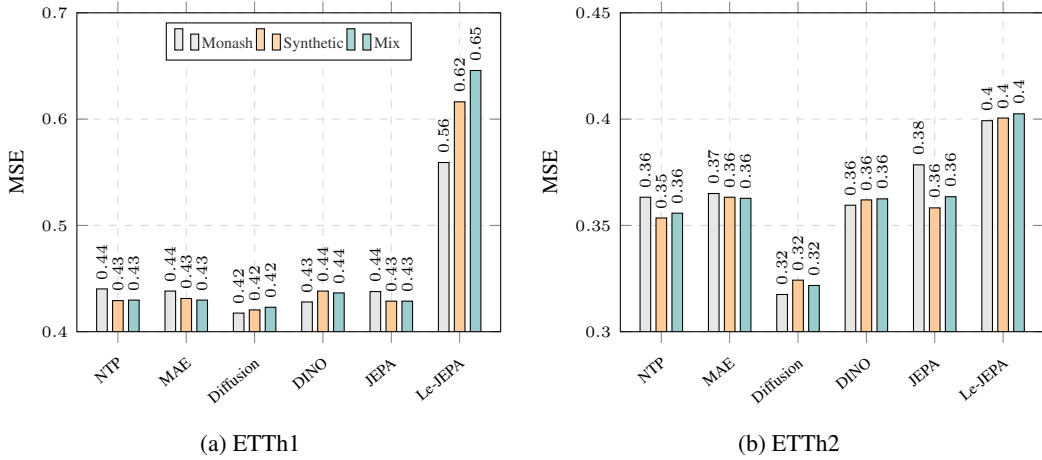


Figure 3: Impact of pre-training data composition on forecasting performance (MSE) for ETTh datasets. Lower is better.

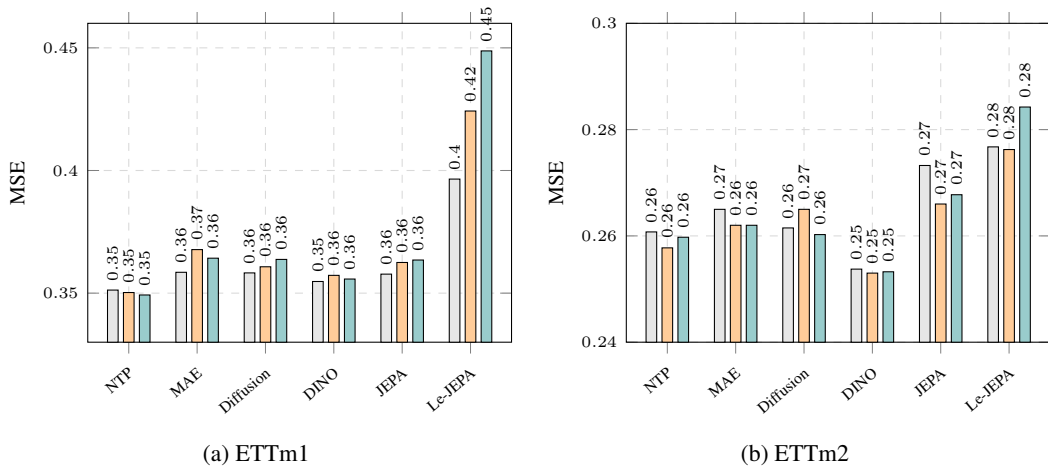


Figure 4: Impact of pre-training data composition on forecasting performance (MSE) for ETTm datasets. Lower is better.

methods. JEPA further achieves the best performance on PSM (0.48), while Diffusion performs best on SMAP (0.31). On SMD, *Generative* methods (NTP) slightly outperform others, achieving the top score (0.53). SWaT remains an outlier, with all methods, including the baseline, performing similarly, indicating limited learnable structure for this dataset. Overall, these results highlight that *Latent*

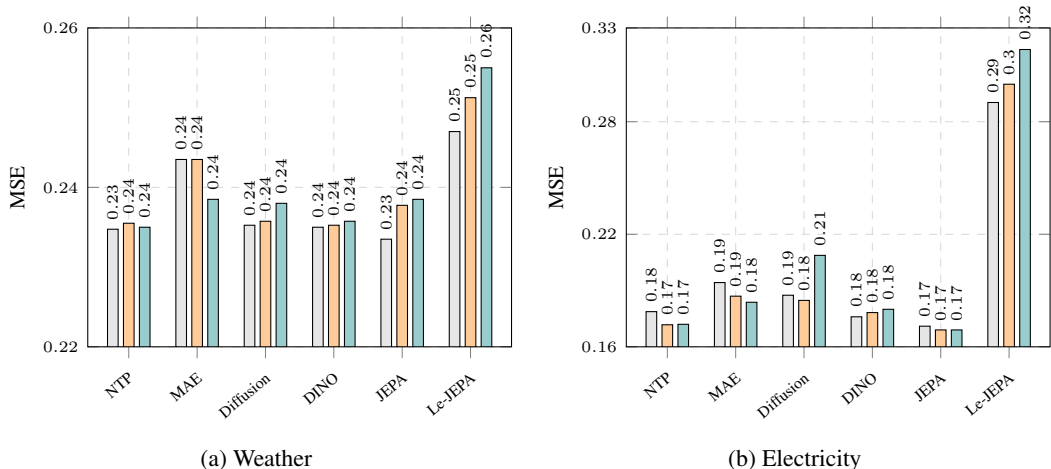


Figure 5: Impact of pre-training data composition on forecasting performance (MSE) for Weather and Electricity. Lower is better.

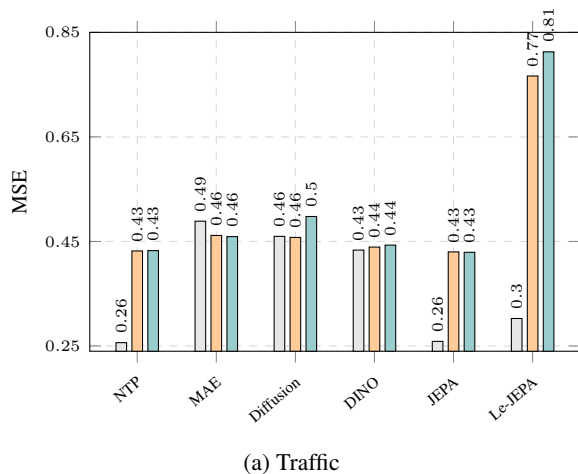


Figure 6: Impact of pre-training data composition on forecasting performance (MSE) for Traffic. Lower is better.

Alignment provides a strong initialization for capturing global anomaly patterns, while *Generative* methods remain competitive on high-entropy signals.

Classification. Table 15 shows that full fine-tuning significantly reshapes the relative ranking between methods. Unlike the linear probing setting, where Le-JEPA and MAE dominated, *Latent Alignment* methods, particularly DINO, emerge as the strongest performers. DINO achieves the best results on multiple datasets, including FaceDetection (0.67), Handwriting (0.15), and UWave (0.81), indicating strong adaptability under end-to-end optimization. At the same time, *Generative* methods remain competitive on specific datasets, with NTP achieving the best performance on JapaneseVowels (0.94) and SCP1 (0.87), and Diffusion achieving the best result on Digits (0.97). Interestingly, the *No Pre-training* baseline remains competitive on simpler datasets such as Ethanol and Heartbeat, suggesting that full fine-tuning can compensate for the lack of pre-training when the underlying structure is simple. Overall, these results indicate that *Latent Alignment* methods provide more flexible and transferable representations when optimized end-to-end.

Forecasting. Table 16 shows that, in contrast to anomaly detection and classification, forecasting performance remains largely insensitive to pre-training under full fine-tuning. The *No Pre-training* baseline consistently achieves the best performance across all datasets and metrics, including ETTh1,

ETTh2, ETTm1, ETTm2, and Weather. While some pre-trained models (e.g., DINO and JEPA) achieve comparable results, none consistently outperform the baseline. In several cases, pre-training even leads to degradation, particularly for Le-JEPA, which shows consistently higher error across all datasets. These findings reinforce the observation that forecasting tasks benefit less from representation learning, and that task-specific optimization dominates performance under full fine-tuning.

Summary. Taken together, these results highlight a clear distinction between tasks. For anomaly detection and classification, pre-training, especially via *Latent Alignment*, provides a strong initialization that can be effectively exploited through full fine-tuning. In contrast, for forecasting, the benefits of pre-training remain limited, even when all parameters are optimized, suggesting that current SSL objectives do not capture the inductive biases required for accurate temporal extrapolation.

Table 14: Full fine-tuning F1 scores on anomaly detection benchmarks. Models are grouped by SSL paradigm; top results per dataset are highlighted in **bold**.

SSL Paradigm	MSL	PSM	SMAP	SMD	SWaT
<i>No Pre-training</i>	0.49	0.14	0.30	0.47	0.11
<i>Generative</i>					
NTP	0.36	0.08	0.29	0.53	0.11
MAE	0.38	0.17	0.27	0.52	0.11
Diffusion	0.53	0.45	0.31	0.51	0.11
<i>Latent Alignment</i>					
DINO	0.29	0.14	0.26	0.51	0.11
JEPA	0.57	0.48	0.31	0.52	0.07
Le-JEPA	0.57	0.45	0.30	0.52	0.03

Table 15: Full fine-tuning accuracy on classification benchmarks. Datasets: **Eth** (EthanolConcentration), **Face** (FaceDetection), **Hand** (Handwriting), **Hrt** (Heartbeat), **Vwl** (JapaneseVowels), **S1/S2** (SCP1/S2), **Dig** (Digits), **UW** (UWave). Top results are highlighted in **bold**.

SSL Paradigm	Eth	Face	Hand	Hrt	Vwl	S1	S2	Dig	UW
<i>No Pre-training</i>	0.29	0.55	0.04	0.72	0.91	0.74	0.56	0.88	0.23
<i>Generative</i>									
NTP	0.20	0.57	0.07	0.66	0.94	0.87	0.46	0.96	0.58
PatchTST	0.29	0.53	0.04	0.72	0.91	0.74	0.56	0.88	0.23
TimeDART	0.24	0.64	0.05	0.63	0.93	0.80	0.53	0.97	0.53
<i>Latent Alignment</i>									
DINO	0.28	0.67	0.15	0.72	0.85	0.85	0.55	0.96	0.81
JEPA	0.27	0.50	0.06	0.57	0.90	0.67	0.54	0.87	0.40
Le-JEPA	0.25	0.62	0.10	0.64	0.89	0.80	0.54	0.96	0.66

A.5 Additional Results Under MLP-based Proving

To evaluate whether the simplicity of the linear probe limits downstream performance, we replace the linear head with a lightweight MLP consisting of a single hidden layer (dimension 512), GELU activation, and dropout of 0.2. All other settings remain unchanged, and the backbone remains frozen.

Results. Tables 19-17 show the results if this experiment for Anomaly Detection, Classification and Forecasting, respectively. Across tasks, introducing an MLP head yields modest and inconsistent improvements. For classification, we observe an average improvement of approximately +3% across methods, with gains for JEPA (+7%), Le-JEPA (+8%), and MAE (+6.5%), while DINO and Diffusion show slight degradation. For anomaly detection, the average improvement is approximately +4%, with stronger gains for JEPA (+20%) and Le-JEPA (+19%), but degradation for Diffusion.

In contrast, forecasting performance slightly degrades when using the MLP head. On average, MSE increases by approximately 1%, and MAE by approximately 0.8% across methods. This trend is consistent across paradigms, including JEPA, DINO, and NTP. Representative results are shown in

Table 16: Full fine-tuning forecasting performance (MSE and MAE) across benchmarks. Datasets: **H1/H2** (ETTH1/2), **M1/M2** (ETTM1/2), **Wth** (Weather). Models are grouped by SSL paradigm; top results (lowest error) per metric and dataset are highlighted in **bold**.

SSL Paradigm	Loss	H1	H2	M1	M2	Wth
<i>No Pre-training</i>	MSE	0.418	0.350	0.348	0.259	0.228
	MAE	0.429	0.392	0.381	0.317	0.264
<i>Generative</i>						
NTP	MSE	0.457	0.375	0.358	0.279	0.233
	MAE	0.454	0.407	0.387	0.330	0.268
MAE	MSE	0.444	0.365	0.355	0.264	0.234
	MAE	0.437	0.404	0.384	0.326	0.269
Diffusion	MSE	0.470	0.347	0.352	0.271	0.229
	MAE	0.457	0.395	0.384	0.325	0.264
<i>Latent Alignment</i>						
DINO	MSE	0.434	0.375	0.354	0.261	0.229
	MAE	0.444	0.408	0.385	0.318	0.265
JEPA	MSE	0.457	0.387	0.357	0.280	0.230
	MAE	0.437	0.418	0.387	0.333	0.265
Le-JEPA	MSE	0.536	0.415	0.389	0.290	0.237
	MAE	0.507	0.438	0.410	0.341	0.272

Discussion. These results indicate that increasing the capacity of the probing head does not fundamentally alter the conclusions of our study. While a more expressive head can slightly improve separability in classification and anomaly detection, it does not compensate for limitations in the learned representations for forecasting. In particular, the marginal performance differences confirm that the observed behavior is primarily driven by the quality and geometry of the pre-trained embeddings rather than by the expressiveness of the downstream head.

Conclusion. Overall, the ablation supports the use of linear probing as a faithful evaluation protocol. Allowing a small MLP head does not change the qualitative ranking between methods nor the conclusion that the pre-training dividend for forecasting remains limited.

Table 17: Forecasting performance (MSE and MAE) using MLP probe. Lower is better; best results per dataset and metric are highlighted in **bold**.

Model	Loss	ETTH1	ETTH2	ETTM1	ETTM2	Weather
JEPA	MSE	0.4444	0.3603	0.3679	0.2738	0.2330
	MAE	0.4474	0.4013	0.3922	0.3292	0.2678
Le-JEPA	MSE	0.5665	0.4075	0.4015	0.2855	0.2426
	MAE	0.5215	0.4327	0.4154	0.3412	0.2787
DINO	MSE	0.4449	0.3685	0.3610	0.2611	0.2297
	MAE	0.4524	0.4027	0.3888	0.3183	0.2665
MAE	MSE	0.4419	0.3906	0.3537	0.2727	0.2308
	MAE	0.4406	0.4219	0.3847	0.3289	0.2667
Diffusion	MSE	0.4302	0.3477	0.3546	0.2670	0.2278
	MAE	0.4369	0.3906	0.3852	0.3211	0.2638
NTP	MSE	0.4324	0.3659	0.3566	0.2640	0.2308
	MAE	0.4412	0.4011	0.3871	0.3216	0.2661
Random	MSE	0.4270	0.3592	0.3562	0.2666	0.2334
	MAE	0.4352	0.3961	0.3868	0.3223	0.2704

A.6 Embedding Analysis

We provide a qualitative analysis of the learned representations using a t-SNE visualization on the *SpokenArabicDigits* dataset (Figure 7). Each point corresponds to an embedded time series instance, colored by its class label.

Since this dataset is used exclusively for classification, the visualization reflects the degree of *class separability* induced by each SSL paradigm. Clear differences emerge between methods.

Table 18: Classification accuracy using MLP probe. Best results per dataset are highlighted in **bold**.

Augmentation	Eth	Face	Hand	Hrt	Vwl	S1	S2	SAD	UW
Jepa	0.2471	0.5199	0.0894	0.6390	0.9324	0.7235	0.5278	0.8558	0.5375
Le-Jepa	0.2471	0.6322	0.2588	0.6390	0.8919	0.8089	0.4778	0.9559	0.8344
DINO	0.2624	0.5077	0.1282	0.7073	0.7676	0.7167	0.5222	0.7522	0.4313
MAE	0.2776	0.5499	0.0682	0.7366	0.9622	0.7952	0.4778	0.9291	0.4750
Diffusion	0.2510	0.5000	0.0812	0.6293	0.9189	0.7133	0.5611	0.8868	0.5563
NTP	0.2624	0.5227	0.1012	0.7122	0.9270	0.7270	0.5444	0.8545	0.6312
Random	0.2928	0.5267	0.0706	0.7268	0.9514	0.7713	0.5000	0.7981	0.4250

Table 19: Anomaly detection performance (F1 score) using MLP probe. Best results per dataset are highlighted in **bold**.

Model	MSL	PSM	SMAP	SMD	SWaT
Jepa	0.5686	0.4095	0.2921	0.5314	0.0302
Le-Jepa	0.5685	0.4511	0.3441	0.5313	0.0300
DINO	0.1882	0.5826	0.1759	0.6087	0.1155
MAE	0.2076	0.5006	0.2424	0.6285	0.1171
Diffusion	0.2473	0.4312	0.1817	0.4916	0.1168
NTP	0.1887	0.5589	0.2491	0.5910	0.1176
Random	0.1773	0.4718	0.2017	0.3578	0.1184

DINO produces well-separated and compact clusters, indicating strong discriminative structure in the embedding space. Le-JEPA also yields highly separable clusters, though with slightly more dispersion, suggesting that its invariance constraints preserve class-level structure while allowing some intra-class variability. JEPA forms coherent but less sharply separated clusters, reflecting a softer organization of the latent space.

In contrast, *Generative* methods exhibit weaker class separation. MAE produces partially clustered representations with noticeable overlap between classes, while NTP shows more entangled embeddings with limited global organization. Diffusion lies between these extremes, forming moderately structured but less compact clusters compared to alignment-based approaches.

Overall, the visualization aligns with the classification results: methods that induce more separable and structured embedding spaces (notably DINO and Le-JEPA) achieve stronger performance on classification benchmarks. As this dataset is used solely for classification, these observations should be interpreted as reflecting representation quality for discriminative tasks rather than general time-series modeling capability.

A.7 Augmentations Ablation Study for DINO and LeJEPA

Setup. To isolate the impact of augmentation design in invariance-based SSL (DINO and Le-JEPA), we evaluate several families of transformations beyond the default DWT-based pipeline. Each augmentation is applied symmetrically to construct dual views and is parameterized by a single magnitude controlling the strength of the transformation. We consider the following families:

- **Galilean & Special-Relativistic:** global temporal rescaling and local Lorentz-style transformations of the form $\gamma(x - v \cdot t)$.
- **Coordinate Transformations:** global polar warps and local rotations in the value–time plane.
- **Hyperbolic Transformations:** global hyperbolic warps and local Möbius shifts on the Poincaré disk.
- **DWT (baseline):** wavelet-based augmentations with structured perturbations in the frequency domain.

Results. Across all tasks, DWT-based augmentations consistently provide the most stable and competitive performance.

SpokenArabicDigits



Figure 7: Embedding Analysis

For **forecasting**, DWT achieves the best or near-best results across datasets (e.g., lowest MSE on ETTH1, ETTM1, and ETTM2), while alternative transformations exhibit inconsistent behavior and often degrade performance. On average, non-DWT augmentations increase forecasting error by approximately 1–3% relative to DWT.

Discussion. These results indicate that the effectiveness of augmentations depends strongly on the alignment between the induced invariances and the underlying signal structure. DWT-based augmentations preserve temporal locality while introducing structured perturbations in the frequency domain, which appears well-suited for forecasting.

In contrast, the alternative transformations introduce more global or nonlinear distortions that are less aligned with the statistical properties of real-world time series. While these transformations are theoretically motivated, they do not translate into effective inductive biases in practice.

Conclusion. Overall, the ablation confirms that the choice of augmentation is critical for invariance-based SSL. DWT-based augmentations provide a robust and well-aligned inductive bias, while alternative transformation families fail to consistently improve performance. This justifies our design choice of using wavelet-based augmentations as the default across all experiments.

A.8 Experimental Setup

To isolate the impact of the SSL paradigm, we employ a unified Transformer encoder backbone across all methods. We vary the architectural capacity by scaling the number of layers $N \in \{2, 4, 8, 12, 24\}$, while maintaining a constant embedding dimension of $D \in \{128, 256\}$ depending on the model family, and a fixed number of attention heads (16 for $D=128$, 8 for $D=256$). All models share the same encoder–predictor structure (8 encoder layers and 4 predictor layers in the default configuration),

Table 20: Forecasting performance (MSE and MAE) across augmentation strategies. Lower is better; best results per dataset and metric are highlighted in **bold**.

Augmentation	Loss	ETTH1	ETTH2	ETTM1	ETTM2	Weather
Galilean & Relativistic	MSE	0.4439	0.3580	0.3578	0.2628	0.2393
	MAE	0.4472	0.3951	0.3857	0.3152	0.2744
Coordinate / Polar	MSE	0.4492	0.3679	0.3549	0.2551	0.2360
	MAE	0.4512	0.4018	0.3825	0.3130	0.2711
DWT	MSE	0.4280	0.3595	0.35475	0.25375	0.2350
	MAE	0.4400	0.40075	0.38425	0.3105	0.2710
Hyperbolic	MSE	0.4535	0.3577	0.3715	0.2703	0.2364
	MAE	0.4518	0.4023	0.3926	0.3314	0.2741

ensuring that differences in performance stem from the SSL objective rather than architectural variations.

A.8.1 Pre-training Datasets

To isolate the impact of data composition on representational anatomy, we define three experimental settings:

- *Real-only*: Restricted to the Monash corpus ($\sim 680\text{K}$ samples). Used to evaluate method efficacy on purely observed, domain-rich data.
- *Synthetic-only*: Restricted to the synthetic corpus ($\sim 2.5\text{M}$ chunks). Tests the ability of SSL paradigms to learn from massive, curated structural primitives.
- *Hybrid (Mixed)*: A mixture of the full Monash set supplemented with $\sim 1.8\text{M}$ synthetic samples to match the 2.5M total scale of the Synthetic-only regime. This setting allows us to observe the synergy between real-world complexity and synthetic scale.

Real-world Dataset. Our pre-training corpus is designed to evaluate how different SSL paradigms scale with data diversity and volume. We utilize the Monash Time Series Forecasting Repository [9], a comprehensive collection spanning diverse domains including finance, weather, and energy. The pre-training set consists of 683,982 training samples, with 77,365 samples for validation. This regime serves as our baseline for high-fidelity observed signals, representing a realistic yet relatively small-scale data scenario.

Synthetic Dataset and Generation Details. To study scaling laws in the absence of domain bias, we generate a large-scale synthetic corpus following the methodology of TimePFN [16]. This dataset consists of 2,512,000 training chunks. These samples provide diverse temporal "building blocks" (e.g., trends and periodicities), but may lack the stochastic variability of real-world data.

The synthetic corpus follows the structural-prior generation scheme introduced in TimePFN [16], which we instantiate using the original scripts with adjusted sequence length and dataset size. Each univariate time series is sampled as a single realization from a Gaussian Process (GP) prior on a uniform temporal grid of length T , where the covariance is constructed by randomly composing base kernels drawn (with replacement) from a fixed bank. The number of kernels per series is sampled uniformly ($K \sim \mathcal{U}\{1, \dots, 5\}$), and kernels are combined via random addition or multiplication operators ($\text{Bernoulli}(\frac{1}{2})$), applied in a left-folded manner.

The kernel bank includes periodic (ExpSineSquared) kernels spanning multiple temporal resolutions (e.g., daily, weekly, yearly), smooth kernels (RBF), multi-scale kernels (Rational Quadratic), linear kernels (Dot-Product), and noise components, enabling diverse temporal patterns such as trends, seasonality, and irregular fluctuations.

Multivariate series are generated using a Linear Coregionalization Model (LCM). A set of latent univariate GP factors is first sampled, and each channel is constructed as a simplex-weighted combination of these latent processes:

$$x_c(t) = \sum_{j=1}^J w_{c,j} f_j(t), \quad w_c \sim \text{Dirichlet}(\alpha \mathbf{1})$$

This induces structured cross-channel correlations with controllable coupling strength. The number of latent factors is sampled from a clipped Weibull distribution, while the Dirichlet concentration parameter controls the sparsity of channel assignments, interpolating between near-independent channels and dense entangled mixtures.

This construction yields synthetic data with controlled temporal structure and inter-channel dependencies, enabling large-scale pre-training while preserving key statistical properties such as multi-scale periodicity and smoothness. While we do not explicitly match higher-order statistics, the generated series exhibit diverse spectral and autocorrelation patterns consistent with real-world signals. However, the simplex-based mixing induces predominantly non-negative correlations, which differs from real benchmarks and represents a known limitation of the generator. We refer to [16] for the full generation algorithm and parameterization.

We follow the default TimePFN generation setup with minor adjustments to sequence length and dataset size. Specifically, each dataset contains $N = 4000$ series of length $T = 2500$. For univariate generation, the number of kernels per series is sampled as $K \sim \mathcal{U}\{1, \dots, 5\}$. The kernel bank consists of 33 atoms, including periodic (ExpSineSquared) kernels at multiple temporal resolutions, RBF and Rational Quadratic kernels with varying length scales, Dot-Product kernels, noise components, and a Constant kernel.

For multivariate generation, we use $C = 160$ channels constructed via a Linear Coregionalization Model with J latent factors sampled from a clipped Weibull distribution. Each latent factor is defined by its own kernel composition, where the number of kernels is sampled independently as $K \sim \mathcal{U}\{1, \dots, 5\}$. Channel mixing weights are drawn from a Dirichlet distribution with concentration parameter $\alpha \sim \mathcal{U}[0.1, 1.0]$, sampled per series. We use the original TimePFN implementation with these parameter settings, modifying only sequence length and dataset size.

A.8.2 Downstream Benchmarks and Metrics

To evaluate the intrinsic quality of the learned representations, we utilize a *linear probing* protocol in which the pre-trained backbone remains frozen and only a single linear head is trained for each downstream task. This approach isolates the contribution of the SSL objective by ensuring that task performance directly reflects the structure of the learned latent space, rather than the capacity of a non-linear decoder to compensate for suboptimal representations. By additionally benchmarking against a frozen, randomly initialized backbone, we quantify the absolute value added by each SSL paradigm, providing a controlled measure of how effectively each method captures fundamental temporal properties such as trend and periodicity in a linearly separable form. We evaluate the frozen representations across three distinct task families:

- *Forecasting*: We consider multivariate sequence-to-sequence prediction, where a fixed context window of length 336 is used to forecast future horizons $\{96, 192, 336, 720\}$. Evaluation is conducted on standard long-term forecasting benchmarks (ETTh1, ETTh2, ETTm1, ETTm2, Weather, Electricity, and Traffic), using Mean Squared Error (MSE) as the primary metric.
- *Classification*: We consider sequence-level classification over labeled time series, evaluated on benchmark datasets including EthanolConcentration, FaceDetection, Handwriting, Heartbeat, JapaneseVowels, SelfRegulationSCP1/2, SpokenArabicDigits, and UWaveGestureLibrary. Performance is measured using classification accuracy.
- *Anomaly Detection*: We consider point-wise anomaly detection in multivariate time series, evaluated on SMD, MSL, SMAP, SWaT, and PSM datasets. These datasets span diverse domains, including satellite telemetry (MSL, SMAP), industrial control systems (SWaT), and large-scale service monitoring (SMD, PSM), exhibiting varying levels of noise, seasonality, and system complexity. Performance is evaluated using F1 score under standard anomaly ratios (0.5%–1.0%). Following the `tslib` protocol, anomaly detection is evaluated in a point-wise setting using fixed percentile-based thresholds (0.5% for SMD and 1.0% for all other datasets), computed over the concatenated train and test anomaly scores without validation-based tuning. We apply the standard point-adjustment (PA) procedure prior to evaluation, such that reported metrics correspond to PA-adjusted point-wise performance. We do not report event-wise metrics (e.g., corrected $F_{0.5}$, saliency, or detection delay), which we leave for future work.

For all tasks, we follow the standard dataset splits and evaluation protocols of `tslib`[18], ensuring consistency with prior work. We include representative state-of-the-art baselines (e.g., PatchTST[14], NTP, TimeDART[21]) and implement them under the same backbone and evaluation setup to ensure a controlled comparison across SSL objectives. Our reproduced results are consistent with those reported in prior work, validating our implementation and enabling a fair assessment of the gains introduced by each pre-training paradigm.

A.8.3 Implementation and Training Details

All models are implemented using the unified Transformer encoder backbone described above, with embedding dimension $D \in \{128, 256\}$ and corresponding attention heads (16 for $D=128$, 8 for $D=256$). The default configuration uses an 8-layer encoder. Method-specific heads are introduced only when required by the SSL objective: in particular, JEPA-style methods employ a dedicated latent prediction head, while reconstruction-based methods use their corresponding decoding heads.

Pre-training is conducted for 20 epochs with batch size 128, using a patch size of 16. Masking follows each method’s design: JEPA and Le-JEPA use multi-block masking (2 blocks with 25% masking per block), while PatchTST follows a standard MAE-style random masking scheme with a 40% ratio. EMA-based methods use a momentum of 0.996. Data augmentations are method-specific: TSDINO employs DWT-based transformations (global soft-thresholding with $\sigma = 0.3$ and local perturbations with noise in $[0.1, 0.3]$), without coefficient zero-out, while Le-JEPA further incorporates Gaussian jitter ($\sigma = 0.05$), amplitude scaling (0.8–1.2), channel dropout ($p = 0.2$), and FFT masking (30%). For forecasting, the linear probe is implemented as a single linear projection applied to the frozen backbone representations. Specifically, given an input context window of length L , the encoder produces a sequence of latent representations, which are passed to a linear head to predict the target horizon H . We follow the standard `tslib` setup for context length, prediction horizon, and stride across all datasets, ensuring consistency with prior work. The probe is trained independently for each dataset and horizon setting.

Optimization uses SGD for JEPA and Adam/AdamW for the remaining models, with OneCycleLR scheduling (5% warmup followed by cosine decay) where applicable. Learning rates are scaled with model size and prediction horizon, ranging from $3e-3$ to $1e-4$ for JEPA-style models and $3e-4$ to $1e-5$ for the remaining baselines.

For downstream linear probing, all tasks are trained for 20 epochs: forecasting uses dataset-specific batch sizes (16–256) and learning rates in $[1e-4, 4e-4]$; classification uses batch size 64 and learning rate $1e-3$; and anomaly detection uses Adam with cosine annealing for 10 epochs with early stopping (patience 3). All experiments are repeated across five random seeds $\{2003, 123, 456, 789, 1337\}$, including end-to-end pretraining and linear probing, and results are reported as averages.

A.8.4 Compute and Train-time Details

All experiments were conducted on NVIDIA RTX PRO 6000 Blackwell GPUs (96GB VRAM, 600W TDP), with each backbone trained on a single GPU. Peak memory usage during pre-training ranged between approximately 8–32GB depending on model depth and dataset. On the Monash collection, pre-training runtime scaled with backbone depth: 2–4 layer models required approximately 2–3 hours, 8-layer models 4–5 hours, 12-layer models 6–7 hours, and 24-layer models around 10 hours per run. Synthetic and mixed-data variants approximately doubled these runtimes, with the deepest 24-layer configurations requiring up to 28 hours.

Downstream evaluation is substantially lighter than pre-training. Classification completes within approximately 20 minutes per dataset, and anomaly detection within 15 minutes per dataset, depending on model depth. Forecasting on smaller benchmarks (ETTm1/2, ETTh1/2, Weather) typically completes within 15 minutes per dataset, while larger datasets scale more significantly: Electricity requires up to 4 hours and Traffic up to 12 hours for the deepest configurations. Memory usage during downstream tasks remains below 20GB for most datasets, increasing to approximately 40GB for Electricity, while certain Traffic configurations may exceed available VRAM (out-of-memory).

A.9 Depth Scaling and Convergence Analysis

Convergence Under Fixed Pre-training Budget. All models are pre-trained for a fixed budget of 20 epochs across all backbone depths, including the deepest 24-layer configurations. Empirically, we observe stable convergence behavior across all evaluated SSL paradigms. Training loss decreases consistently in early epochs and plateaus thereafter, with no evidence of instability or divergence even for deep models.

Model selection is based on the best validation checkpoint rather than the final epoch. Across methods, peak validation performance typically occurs before the full budget is exhausted, most commonly around epochs 15–16. This indicates that the fixed 20-epoch budget is sufficient for convergence and does not disadvantage deeper models.

Training Dynamics for Deep Models. Figure 8 presents representative training curves for 24-layer models pre-trained on the Synthetic dataset for three paradigms: DINO, MAE, and NTP. All methods exhibit rapid initial improvement followed by saturation. DINO converges quickly within the first few epochs, MAE shows a gradual but consistent decrease, and NTP stabilizes early with minor fluctuations. Improvements beyond epoch 15 are marginal across all methods.

Implications for Depth Scaling. These results support our main finding that performance saturation at 8–12 layers is not caused by insufficient training. Even at 24 layers, models converge within the allocated budget, suggesting that the observed saturation reflects limits of the learned representations rather than optimization constraints. While we do not perform compute-normalized scaling (e.g., matched optimization steps), the consistent convergence behavior across depths indicates that additional training would likely yield only marginal improvements.

Finally, deeper models incur substantially higher computational cost. For example, 24-layer models trained on Synthetic or Mixed data require up to 28 hours per run (Appendix A.8.3), reinforcing the practical relevance of the observed saturation point.

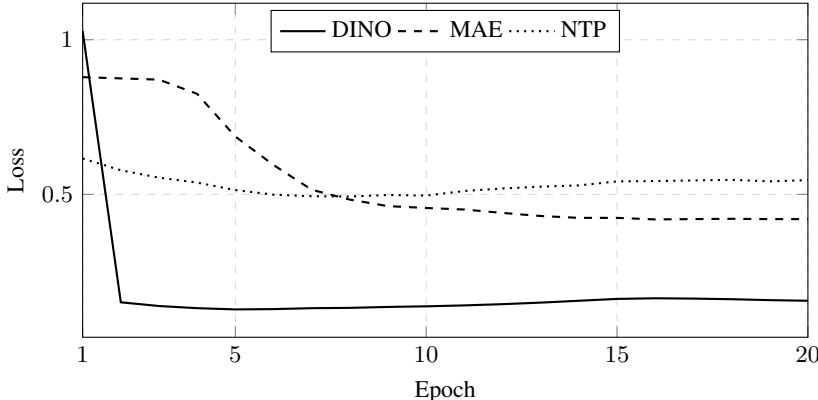


Figure 8: Training loss curves for 24-layer models pre-trained on the Synthetic dataset. All methods exhibit rapid convergence within the first epochs followed by saturation.

A.10 Details and Extended Analysis: LeJEPa and DINO

A.10.1 Le-JEPa

Architecture and Objective. Le-JEPa adopts a dual-view training scheme in which two complementary augmentations of the same input are constructed: a *clean* view and a *hard* view derived via DWT-based perturbations. Both views are processed by a shared encoder, producing embeddings \mathbf{z}_g (clean/global) and \mathbf{z}_a (augmented). The learning objective combines cross-view invariance with a distributional regularization term:

$$\mathcal{L}_{\text{Le-JEPa}} = (1 - \lambda) \|\bar{\mathbf{z}}_g - \mathbf{z}_a\|_2^2 + \lambda T(\mathbf{z}_m),$$

where $\bar{\mathbf{z}}_g$ denotes the batch-wise centroid of the global-view embeddings and $T(\cdot)$ denotes the SIGReg regularizer. This formulation eliminates the need for teacher–student architectures, stop-gradient operations, or EMA updates, and instead relies on explicitly shaping the embedding distribution.

SIGReg Implementation. Le-JEPA employs a Sliced Gaussianity Regularization (SIGReg) term based on the Epps–Pulley test. At each training step, $M = 1024$ random projection directions are sampled on the unit sphere in \mathbb{R}^D (Gaussian vectors with ℓ_2 normalization, seeded by the global step for consistency across workers). Embeddings are projected onto each direction, producing scalar distributions.

For each projection, the empirical characteristic function is computed:

$$\hat{\phi}(t) = \frac{1}{N} \sum_{n=1}^N e^{it\langle a, x_n \rangle},$$

and compared against the standard normal characteristic function $\exp(-t^2/2)$. The squared residual is evaluated over a fixed grid of 17 points in $t \in [-5, 5]$, weighted by $\exp(-t^2/2)$, integrated numerically, scaled by batch size, and averaged across projections.

Training Stability. Two implementation choices are critical for stable training. First, SIGReg is computed in float32, as mixed-precision evaluation of complex exponentials leads to numerical instability. Second, the regularization weight is kept small ($\lambda = 0.008$), ensuring that the invariance term dominates the optimization and SIGReg acts as a weak anti-collapse prior. Larger values (e.g., $\lambda = 0.05$) were found to over-regularize the embeddings and degrade performance on time-series data.

Embedding Geometry. The effect of SIGReg on representation geometry is illustrated in Figure 9. Random one-dimensional projections (left panel) closely follow a standard normal distribution across directions, confirming that Gaussianity is achieved beyond coordinate-wise marginals. The covariance spectrum (middle panel) shows that most embedding dimensions are driven toward unit variance, indicating a near-isotropic representation with high effective rank. Despite this strong regularization, PCA projections (right panel) reveal that class-level structure remains separable, indicating that discriminative information is preserved under the Gaussianity constraint.

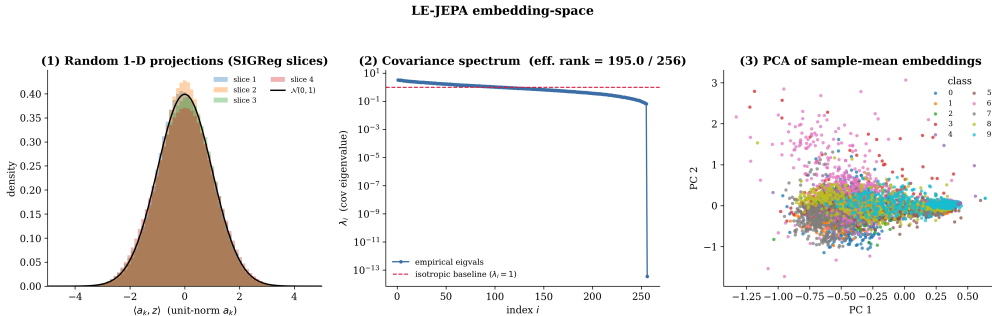


Figure 9: SIGReg-induced embedding geometry for Le-JEPA on the SpokenArabicDigits dataset. (1) Random 1-D projections show strong alignment with a standard normal distribution across directions, confirming Gaussianity beyond coordinate-wise marginals. (2) Covariance spectrum indicates near-isotropic structure, with most eigenvalues close to unity and an effective rank of approximately 195/256. (3) PCA visualization of sample-mean embeddings demonstrates that class-level structure remains separable despite strong distributional regularization.

Impact on Forecasting. Our analysis indicates that the observed degradation in forecasting performance is primarily driven by the isotropic geometry induced by SIGReg, rather than by the DWT-based augmentations. Enforcing Gaussianity across projection directions suppresses directional variance and scale information, which are critical for regression-based tasks. While this structure improves linear separability for classification, it reduces the magnitude-sensitive information required for accurate temporal extrapolation.

In contrast, similar DWT-based augmentations are employed in DINO-style models without causing comparable degradation, suggesting that invariance alone is not the dominant factor. Instead, SIGReg imposes a global distributional constraint that reshapes the embedding space, creating a trade-off between separability-oriented and regression-relevant representations.

Summary. Le-JEPA provides a principled mechanism for preventing collapse and enforcing structured embeddings without relying on teacher networks. However, the induced isotropic geometry, while beneficial for classification and clustering, can be detrimental for forecasting tasks that rely on directional and scale-sensitive information.

A.10.2 DINO

DINO contrasts with Le-JEPA by enforcing invariance through teacher–student distillation rather than via explicit constraints on the embedding distribution.

Architecture and Objective. DINO follows a self-distillation paradigm based on asymmetric views of the same input. Two augmented views are constructed, analogous to a *target* and a *context* view, using DWT-based transformations of varying strength. These views are processed by a student–teacher architecture, where the student network is trained to match the output distribution of the teacher.

The training objective minimizes the cross-entropy between the teacher and student output distributions:

$$\mathcal{L}_{\text{DINO}} = - \sum p_{\theta'}(\mathbf{x}_{\text{teacher}}) \log p_{\theta}(\mathbf{x}_{\text{student}}),$$

where θ' denotes the teacher parameters and θ the student parameters. Unlike reconstruction-based objectives, DINO aligns representations at the distribution level, encouraging consistency across views without explicit prediction of input structure.

Teacher–Student Dynamics. A key component of DINO is the use of an exponential moving average (EMA) teacher. The teacher parameters are updated as a momentum-based average of the student parameters, ensuring a slowly evolving target representation. To prevent collapse, the teacher outputs are further stabilized through two mechanisms: (i) *centering*, which subtracts a running mean from the logits, and (ii) *sharpening*, which applies a low-temperature softmax to produce peaked target distributions.

Together, these mechanisms ensure that the student is trained against a stable and informative target signal, avoiding trivial constant representations while encouraging consistency across augmented views.

Augmentations and Invariances. In our setting, DINO operates on dual DWT-based views that differ in augmentation strength, encouraging the model to learn invariances to structured perturbations in the signal. Beyond wavelet-based augmentations, we evaluated a range of physics- and geometry-motivated transformations designed to encode alternative invariances for time-series representations.

The mechanical family comprises a Galilean rescaling of the time axis, an additive linear drift, a rotation in the value–time plane, and a Lorentz boost of the form $\gamma(x - v \cdot t)$ acting on the signal as a worldline. The geometric family comprises a polar-coordinate warp, a tanh amplitude compression, and a Möbius shift on the Poincaré disk. Each transformation is controlled by a single magnitude parameter sampled per view and was evaluated independently of the wavelet pipeline.

Empirically, DWT-based augmentations consistently outperform alternative transformation families across forecasting and anomaly detection tasks, and remain competitive in classification (see Appendix A.7). In contrast, the evaluated physics- and geometry-motivated transformations do not yield consistent improvements and often degrade performance. This suggests that not all theoretically motivated invariances translate into useful inductive biases for time-series representation learning. A detailed quantitative comparison across augmentation families is provided in Appendix A.7.

Representation Behavior. DINO encourages the encoder to capture multi-scale structural invariants by aligning representations across differently perturbed views. Unlike Le-JEPA, which explicitly enforces a Gaussian latent structure, DINO imposes an implicit regularization through the

teacher–student dynamics. As a result, the learned embeddings retain richer directional variance and anisotropy, which is beneficial for downstream regression tasks such as forecasting.

This difference in geometric bias is reflected in our empirical results: DINO remains competitive on forecasting benchmarks, in contrast to Le-JEPA, which exhibits degradation due to its stronger isotropy constraint. At the same time, DINO achieves strong performance in classification tasks, indicating that invariance-based alignment provides a balanced trade-off between separability and representational richness.

Summary. DINO provides a robust self-distillation framework for learning invariant representations without explicit distributional constraints. Its combination of EMA-based targets and augmentation-driven alignment yields stable training and versatile representations across tasks.

Taken together, these results highlight a fundamental distinction between the two paradigms: explicit distributional regularization (Le-JEPA) enforces strong geometric structure at the cost of regression-relevant information, while implicit invariance (DINO) preserves richer representations at the cost of weaker control over embedding geometry.